

兰州理工大学

科研成果汇总

| | |
|--------|--------------------------|
| 学 号: | 201081191003 |
| 研 究 生: | 李锦键 |
| 导 师: | 王兴贵 教授 |
| 研究方向: | 新能源发电控制技术 |
| 论文题目: | 微源半桥变流器串联微电网 并网系统控制研究 |
| 学 科: | 可再生能源发电与智能电网 |
| 学 院: | 电气工程与信息工程学院 |
| 入学时间: | 2020 年 9 月 |

2025 年 5 月 29 日

目 录

| | |
|--|----|
| 1. 论文检索报告..... | 1 |
| 2. 论文录用证明..... | 4 |
| 3. Wang Xinggui, Li Jinjian, Guo Qun, Wang Hailiang, Ding Yingjie. Parameter design of half-bridge converter series Y-connection microgrid grid-connected filter based on improved PSO-LSSVM[J]. International Transactions on Electrical Energy Systems, 2023: 9534004. (SCI: WOS:000943372900001)..... | 6 |
| 4. 李锦键, 王兴贵, 李昱, 丁颖杰, 薛晟. 基于波动量自适应补偿的 HCSY-MG 系统并网电流模型预测控制[J]. 控制理论与应用. (EI 源 刊, 已录用)..... | 19 |
| 5. 李锦键, 王兴贵, 丁颖杰. 基于改进 PPO 的 HCSY-MG 并网系统 分布式混合储能充放电优化控制[J/OL]. 电源学报, 2024: 1-13. (CSCD 源刊, 已录用)..... | 29 |



机构: 兰州理工大学

姓名: 李锦键 [201081191003]

著者要求对其在国内外学术出版物所发表的科技论著被以下数据库收录情况进行查证。

检索范围:

- 科学引文索引 (Science Citation Index Expanded): 1900年-2025年
- 工程索引 (Engineering Index): 1884年-2025年

检索结果:

| 检索类型 | 数据库 | 年份范围 | 总篇数 | 第一作者篇数 | 第二作者篇数 |
|----------|--------------|------|-----|--------|--------|
| SCI-E 收录 | SCI-EXPANDED | 2023 | 1 | | 1 |
| EI 收录 | EI-Compendex | 2022 | 1 | 1 | |

End



委托人声明:

本人委托兰州理工大学图书馆查询论著被指定检索工具收录情况, 经核对检索结果, 附件中所列文献均为本人论著, 特此声明。

作 者 (签字): 李锦键

完 成 人 (签字): 安宇五

完 成 日 期 : 2025年3月24日

完成单位 (盖章): 兰州理工大学图书馆信息咨询与学科服务部

(本检索报告仅限校内使用)



图书馆

文献检索报告
SCI-E 收录

兰州理工大学图书馆 LUTLIB

报告编号: R2025-0231 SCI-E 收录

数据库: 科学引文索引 (Science Citation Index Expanded)
时间范围: 2023年作者姓名: 李锦键
作者单位: 兰州理工大学检索人员: 安宇王
检索日期: 2025年3月24日

检索结果: 被 SCI-E 收录文献 1 篇

| # | 作者 | 地址 | 标题 | 来源出版物 | 文献类型 | 入藏号 |
|----|--|--|---|--|--------------|---------------------|
| 1 | Wang, XG; Li, JJ; Guo, Q; Wang, HL; Ding, YJ | [Wang, Xinggui; Li, Jinjian; Guo, Qun; Wang, Hailiang; Ding, Yingjie] Lanzhou Univ Technol, Coll Elect Engn & Informat Engn, Lanzhou 730050, Peoples R China. | Parameter Design of Half-Bridge Converter Series Y-Connection Microgrid Grid-Connected Filter Based on Improved PSO-LSSVM | <i>INTERNATIONAL TRANSACTIONS ON ELECTRICAL ENERGY SYSTEMS</i> 2023, 2023, 9534004. | J Article | WOS:000943372900001 |
| 合计 | | | | | | 1 |



图书馆

文献检索报告
EI 收录

兰州理工大学图书馆 LUTLIB

报告编号: R2025-0231 EI 收录

| 数据库: 工程索引 (Engineering Index) 时间范围: 2022年 | | 作者姓名: 李锦键 作者单位: 兰州理工大学 | | 检索人员: _____ 检索日期: 2025年3月24日 | | |
|--|---|--|--|---|----------------------|--------------------|
| 检索结果: 被 EI 收录文献 1 篇 | | | | | | |
| # | 作者 | 地址 | 标题 | 来源出版物 | 文献类型 | 入藏号 |
| 1 | Li, Jinjian; Wang, Xinggui; Yang, Weiman; Zhao, Lingxia | College of Electrical Engineering and Information Engineering, Lanzhou University of Technology, Lanzhou | CSP station output power short-term forecast based on improved RNN-DBN 基于改进递归深度信念网络的CSP电站短期出力预测 | Taiyangneng Xuebao/Acta Energiae Solaris Sinica 2022, 43 (7): 225-232. | Journal article (JA) | 202231125 26513 |
| 合计 | | | | | | 1 |



论文录用证明

李锦键，王兴贵，李昱，丁颖杰，薛晟先生/女士：

尊稿“基于波动量自适应补偿的 HCSY-MG 系统并网电流模型预测控制”经本刊审查，决定录用。

特发此学术论文录用证。

《控制理论与应用》编辑部
2025-02-26



录用通知

尊敬的 李锦键, 王兴贵, 丁颖杰 作者:

您好! 首先祝贺您的稿件《基于改进 PPO 的 HCSY-MG 并网系统分布式混合储能充放电优化控制》(编号 JOPS-2024-0473) 已被本刊正式录用!

为了更好地解决出版时滞问题, 我刊编辑部将于近期在“中国知网”学术期刊优先数字出版平台对其进行发布, 印刷版出版时间待定。
特此通知!

感谢您对本刊的支持, 欢迎再次来稿!

此致

敬礼!



第一作者: 李锦键, 兰州理工大学电气工程与信息工程学院, 730050

中国电源学会—《电源学报》编辑部

地址: 天津市南开区黄河道 467 号大通大厦 10 层 (300110)

电话: 022-27686327 传真: 022-27687886

网址: www.jops.cn E-mail: jops@cpss.org.cn

Research Article

Parameter Design of Half-Bridge Converter Series Y-Connection Microgrid Grid-Connected Filter Based on Improved PSO-LSSVM

Xinggui Wang, Jinjian Li , Qun Guo, Hailiang Wang, and Yingjie Ding

College of Electrical Engineering and Information Engineering, Lanzhou University of Technology, Lanzhou 730050, China

Correspondence should be addressed to Jinjian Li; lijinjian0326@163.com

Received 23 November 2022; Revised 4 February 2023; Accepted 9 February 2023; Published 24 February 2023

Academic Editor: Arvind R. Singh

Copyright © 2023 Xinggui Wang et al. This is an open access article distributed under the Creative Commons Attribution License, which permits unrestricted use, distribution, and reproduction in any medium, provided the original work is properly cited.

The half-bridge converter series Y-connection microgrid (HCSY-MG) is a new type of series microgrid. In order to reduce the harmonic content in HCSY-MG grid-connected current and at the same time simplify the parameter design process of the LCL filter, this study proposed an LCL filter parameter design method based on an improved particle swarm optimization-least squares support vector machine (PSO-LSSVM) by analyzing the harmonic characteristics of the HCSY-MG grid-connected current. In addition, to enhance the convergence speed of PSO-LSSVM, the inertia factor during its parameters' update is made to adjust adaptively according to the direction of two consecutive parameter changes to constitute an improved PSO-LSSVM. Through simulation and comparative analysis, it is demonstrated that the improved PSO-LSSVM can enhance the convergence speed; the proposed filter parameter design method can effectively reduce the harmonic content in the HCSY-MG grid-connected current and is simpler and more comprehensive than the existing design method.

1. Introduction

In the context of global environmental pollution and primary energy shortage, microgrid, which was proposed at the beginning of the 21st century, has received unprecedented attention [1, 2]. The microgrid structures that today can be classified as AC, DC, and hybrid AC-DC are based on the main bus supply [3]. Among them, the AC microgrids are the most widely used and valuable for research because they supply the same power as the electric system. However, the parallel access method used by each grid-connected converter in the AC microgrid generates a large amount of loop current within the system, which makes the utilization of renewable energy low, and also, the stability and power quality of the system is poor [4, 5].

In order to solve the inherent problems in traditional AC microgrids, some scholars have proposed series structured microgrids with the topology, including series micropower grids and modular multilevel converter microgrids [6, 7]. Due to the special topology of the series microgrid, its harmonics are mainly distributed around integer multiples of the equivalent carrier frequency, so most of the existing

parameter design methods for grid-connected filters will no longer be applicable. This study will take a half-bridge converter series Y-connection microgrid (HCSY-MG) as the research object and propose a grid-connected LCL filter parameter design method applicable to series-connected microgrids to simplify the design process while reducing the harmonic content in the grid-connected current. The HCSY-MG system has the advantages of simple control, no loop current, and higher utilization of renewable energy due to the topology of Y-connection, so it is meaningful to study the parameter design method of its grid-connected filter and can provide some references for the grid-connected operation of the series microgrid.

In microgrids, active and passive power filters are generally used to reduce the amplitude of harmonics in the system. In the literature [8–10], corresponding active filter optimization design methods are proposed for different types of microgrids, which effectively improve the power quality of the AC busbar. Compared to the active filter, the passive filter is more suitable for scenarios with a higher power. Because the HCSY-MG system already contains a large number of electric power components, the use of an

active filter will further increase the difficulty of controlling the system; this study will use the passive LCL grid-connected filter. The LCL filter is widely used as the interface between a microgrid converter and power system because of its better filtering effect. However, the topology of its third-order system makes the design of component parameters a research focus and difficulty [11]. Regarding the parametric design methods of LCL filters, there are mainly traditional design methods, graphical analysis methods, optimized parameters methods, and multivariate system of equations methods. Among them, the conventional design method for LCL filter parameters is given by literature [11], where the parameters of each element are designed sequentially subjected to constraints. Through theoretical analysis, literature [12, 13] proposed a graph containing the LCL filter parameters with the filtering effects and then used graphical analysis to obtain a parameter design and optimization method. In literature [14], a method based on a multivariate system of equations is given to obtain the design values of each element parameter by solving the LCL filter parametric equation, which has a strong generality. In addition to the abovementioned three methods, the most commonly used LCL filter parameter design method is the parameter optimization method. For example, there are minimization of energy storage element values, minimization of damping resistance losses, and minimization of total inductance values [15–17]. The literature [18] proposed a design approach based on multiobjective optimization, where the objectives considered include a filter inductance ratio to minimize total filter inductance and filter admittance to meet grid regulation and characteristic impedance for low current stress of switch stack. Regarding optimization algorithms, the genetic algorithm and its improvements, adaptive weight particle swarm algorithms, as well as adaptive multipopulation-modified nondominated ranking genetic algorithm combined with criteria importance interrelationship and similarity ranking preference technique have been successfully applied to the optimal design of parameters for grid-connected LCL filters [19–21]. Besides, a combination of the previous methods can be used to make the designed LCL filter parameters better. For example, based on the causes of harmonics generated by the converter, literature [22] developed an estimation model of the current total harmonic distortion (THD), and the values of the parameters of each element of the LCL filter were obtained with the current THD minimum as the optimization objective. Literature [23] based on the traditional graphical method and using the Bode diagram of the main transfer function as an entry point, the relationship between each component parameter of the filter and the design requirement was analyzed to first determine the approximate range of values for each parameter and then determine the optimal values by the Gray wolf optimization algorithm. Literature [24] analyzed the high-frequency harmonics of inverter output voltage in detail and constructed multiobjective optimization function that included five optimization objectives. Then, combined with the particle swarm optimization, a screening method is

proposed to realize the multiobjective optimization process of designing LCL filter parameters.

For the mentioned problems that require experience, iterative trials, and optimization, machine learning models can achieve better solutions through their ability to extract deep and high-order information from the data. The least square support vector machine (LSSVM) belonging to machine learning has been successfully applied to short-term load forecasting in the power system, photovoltaic output power forecasting, and orbital circuit fault diagnosis due to its ability to show superior modeling and prediction in applications with small sample size, nonlinearity, and low dimensionality and can be improved according to specific objects [25–27].

In summary, most of the existing LCL filter parameter design methods are proposed based on common two-level converters, which are not necessarily applicable to the HCSY-MG system or even to the series-connected microgrids, so an LCL filter parameter design method applicable to the HCSY-MG system is studied in this article. Then, the parameter design method of an HCSY-MG grid-connected LCL filter based on improved PSO-LSSVM proposed in this study is based on the analysis of the grid-connected current characteristics of the HCSY-MG system, which utilized the PSO-LSSVM algorithm in machine learning and made its inertia factor adaptively adjusted during particle velocity update to obtain an improved PSO-LSSVM model. The LCL filter design method proposed in this study can flexibly adjust the input vector to be more suitable for the target system according to the actual application while avoiding the iterative trial of relying on engineering experience, which can make the design process more convenient. Through simulation, it is verified that the LCL filter designed by this method can effectively improve the power quality of grid-connected current, reduce the harmonic content in grid-connected current, and meet the corresponding constraint requirements.

2. System Structure and Grid-Connected Current Characteristics

2.1. Structure of the HCSY-MG System. The HCSY-MG system is based on the existing series microgrid and uses generation submodule (GM) as the basic unit, which is connected in a series structure with Y-connection to form a three-phase converter link and then connected to the AC bus through the LCL grid-connected filter. The topology of the GM is shown in Figure 1, and the topology of the HCSY-MG is shown in Figure 2.

In Figure 1, ES is the energy storage, R is the energy dissipation resistor, C is the voltage regulator capacitor, u_{dc} is the half-bridge converter DC side bus voltage, i_{dc} is the half-bridge converter output current, and $S_{1,2}$ is the power switching device. In the GM topology, both the ES and C are used to stabilize the bus voltage on the DC side of the microsource, where the ES also provides some damping for the system to ensure stable and safe operation of the HCSY-MG system. When the microsource output power is greater than the rated output power, the remaining energy

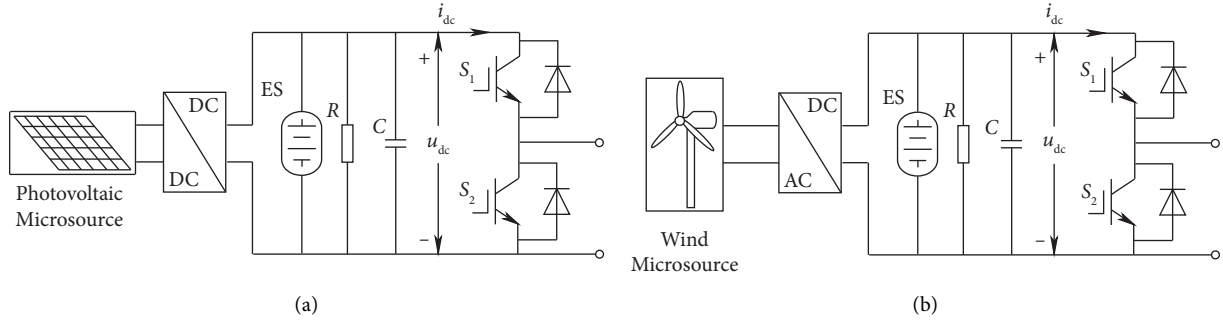


FIGURE 1: Topology structure of GM. (a) Photovoltaic GM topology and (b) wind power GM topology.

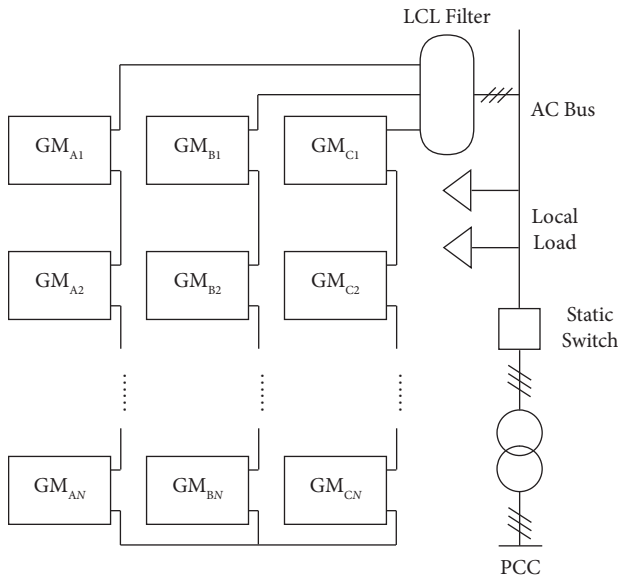


FIGURE 2: Topology structure of HCSY-MG.

can be stored in ES to avoid waste. When the microsource output power is less than the rated output power, the energy stored in ES can be released to compensate for the lack of microsource output power. In addition, the C mitigates the effect of small fluctuations in microsource output power on the HCSY-MG system output and the effect of small fluctuations in load or grid power on the microsource side. In Figure 2, PCC is the point of common coupling.

From Figure 2, the HCSY-MG system consists of N GMs per phase, and the three-phase converter link includes a total of $3N$ GMs. This system can adjust the system output voltage according to the actual application through adjusting the number of converter link output levels by flexibly selecting the number of GMs in each phase. By equating the N series GMs of each phase as the controlled voltage source, the equivalent circuit of the system in a grid-connected mode can be obtained as shown in Figure 3.

In Figure 3, O is the connection point of the three-phase series converter link, u_{XO} is the output voltage of phase X ($X = A, B$, and C) of the series converter link, respectively, R_l is the line equivalent resistance of each phase of the series converter link, L_c is the converter-side filter inductor, R_f is

the filter damping resistor, C_f is the filter capacitor, L_g is the grid-side filter inductor, R_g is the grid line equivalent resistance, i_{eX} is the grid current of each phase X , e_X is the grid voltage of each phase X , and N is the grid neutral point.

2.2. Analysis of Grid-Connected Current Characteristics. When the HCSY-MG system is in stable operation, it is known from the system topology that the double Fourier expansion of the output voltage of the i th GM under the carrier phase shifting Sine pulse width modulation (CPS-SPWM) strategy for phase A, for example, can be given by [28]

$$u_A(i) = \frac{u_{dcA}(i)}{2} + \frac{Mu_{dcA}(i)}{2} \sin(\omega_0 t + \varphi_A) + \sum_{m=1}^{\infty} \sum_{n=-\infty}^{\infty} \frac{2u_{dcA}(i)}{m\pi} J_n\left(\frac{Mm\pi}{2}\right) \sin\left(\frac{(m+n)\pi}{2}\right) \cos \cdot \left[m\left(\omega_c t + (i-1)\frac{2\pi}{N}\right) + n(\omega_0 t + \varphi_A) \right], \quad (1)$$

where $u_A(i)$ is the output voltage of the i th GM of phase A, $u_{dcA}(i)$ is the DC chain voltage of the i th GM of phase A, M denotes the modulation depth, ω_0 is the modulating wave angular frequency, φ_A is the initial phase angle of the phase A modulated wave, m is the harmonic order of the carrier wave ($m = 1, 2, \dots$), n is the harmonic order of the reference wave ($n = 0, \pm 1, \pm 2, \dots$), $J_n(x)$ refers to the Bessel coefficient of order n and argument x , ω_c is the angular frequency of the triangular carriers, and N is the total number of microsources per phase.

So, the output voltage of phase A, u_{AO} , can be expressed as

$$u_{AO} = \sum_{i=1}^N u_A(i) = \frac{u_{dcA}}{2} + \frac{M \cdot u_{dcA}}{2} \sin(\omega_0 t + \varphi_A) + \sum_{m=N, 2N, \dots}^{\infty} \sum_{n=-\infty}^{\infty} \frac{2u_{dcA}}{m\pi} J_n\left(\frac{Mm\pi}{2}\right) \sin\left(\frac{(m+n)\pi}{2}\right) \cdot \cos[m\omega_c t + n(\omega_0 t + \varphi_A)], \quad (2)$$

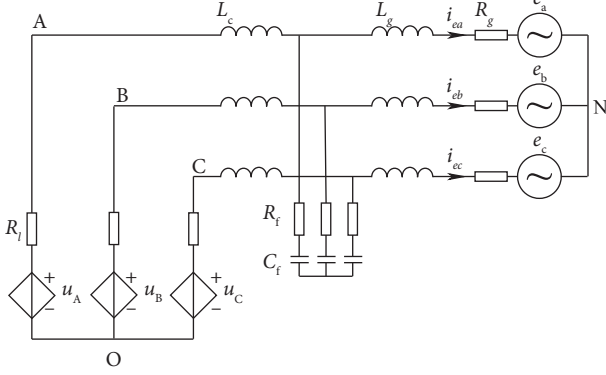


FIGURE 3: System equivalent circuit of the HCSY-MG grid-connected mode.

where $u_{dcA} = \sum_{i=1}^N u_{dcA}(i)$ is the equivalent DC bus voltage of phase A on the converter-side of the system.

Let $\varphi_A = 0$, $\varphi_B = -2\pi/3$, and $\varphi_C = 2\pi/3$, then the output voltage u_{AB} can be expressed as

$$u_{AB} = u_{AO} - u_{BO} = \left(\frac{u_{dcA}}{2} - \frac{u_{dcB}}{2} \right) + M \left(\frac{u_{dcA}}{2} + \frac{u_{dcB}}{4} \right) \cdot \sin \omega_0 t + \frac{\sqrt{3}}{4} M \cdot u_{dcB} \cdot \cos \omega_0 t + \sum_{m=N, 2N, \dots}^{\infty} \sum_{n=-\infty}^{\infty} \frac{2\sqrt{a^2 + b^2}}{m\pi} J_n \left(\frac{Mm\pi}{2} \right) \sin \left(\frac{(m+n)\pi}{2} \right) \sin (m\omega_c t + n\omega_0 t + \psi), \quad (3)$$

where $a = u_{dcB} \sin (m\theta - 2\pi n/3)$; $\psi = \arctan b/a$; $b = u_{dcA} - u_{dcB} \cos (m\theta - 2\pi n/3)$; θ is the carrier phase shift angle.

At this point, let $u_{dcA} = u_{dcB} = u_{dcC} = u_{dc}$, $\theta = 0^\circ$, then the voltage u_{AB} can be expressed as

$$u_{AB} = u_{AO} - u_{BO} = \frac{\sqrt{3}}{2} M u_{dc} \sin \left(\omega_0 t + \frac{\pi}{6} \right) + \sum_{m=N, 2N, \dots}^{\infty} \sum_{n=-\infty}^{\infty} \frac{(-1)^n 4u_{dc}}{m\pi} J_n \left(\frac{Mm\pi}{2} \right) \sin \left(\frac{(m+n)\pi}{2} \right) \sin \left(\frac{n\pi}{3} \right) \sin \left(m\omega_c t + n\omega_0 t - \frac{n\pi}{3} \right). \quad (4)$$

When the local load or parallel network adopts the Δ -connection method, the connection point directly receives the u_{AB} , u_{BC} , and u_{CA} . If the current follows the voltage, the output current of phase A of the system can be expressed as

$$i_{ea} = I_{ea} \sin \left(\omega_0 t + \frac{\pi}{6} + \varphi \right) + i_{eah}, \quad (5)$$

where I_{ea} is the amplitude of the fundamental component of the output current, φ is the power factor angle, and i_{eah} is the high-frequency harmonic component.

When the local load or parallel network adopts the Y-connection method, the connection point does not directly receive the u_{AB} , u_{BC} , and u_{CA} . At this point, through the KVL equation, the output voltage can be expressed as

$$\begin{cases} u_{AN} = \frac{2u_{AO} - u_{BO} - u_{CO}}{3} = \frac{u_{AB} - u_{CA}}{3}, \\ u_{BN} = \frac{2u_{BO} - u_{AO} - u_{CO}}{3} = \frac{u_{BC} - u_{AB}}{3}, \\ u_{CN} = \frac{2u_{CO} - u_{AO} - u_{BO}}{3} = \frac{u_{CA} - u_{BC}}{3}, \end{cases} \quad (6)$$

where u_{XN} is the voltage between the output point of phase X ($X = A, B, C$) of the series converter link and the local load or the neutral point of the power system.

Furthermore, continuing with the example of phase A, the voltage u_{AN} can be expressed as

$$u_{AN} = u_{ANf} + u_{ANh} = \frac{1}{2} M u_{dc} \sin (\omega_0 t) + \sum_{m=N, 2N, \dots}^{\infty} \sum_{n=\pm 1, \pm 3, \dots}^{\infty} \frac{4u_{dc}}{m\pi} J_n \left(\frac{Mm\pi}{2} \right) \sin \left(\frac{(m+n)\pi}{2} \right) \cdot \cos \left(\frac{n\pi}{3} \right) \sin (m\omega_0 t + n\omega_c t), \quad (7)$$

where u_{ANf} and u_{ANh} are the fundamental and harmonic components of u_{AN} , respectively.

So, the fundamental component of the output voltage u_{AN} can be expressed as

$$u_{ANf} = \frac{1}{2} M u_{dc} \sin (\omega_0 t) = u_{AOf} - \frac{1}{2} u_{dc}, \quad (8)$$

where u_{AOf} is the fundamental component of u_{AO} .

If the current follows the voltage, then the output current of phase A of the system at this time can be expressed as

$$i_{ea} = I_{ea} \sin (\omega_0 t + \varphi) + i_{eah}. \quad (9)$$

From the aforementioned mathematical expressions, the characteristics of the grid-connected current of the HCSY-MG system can be obtained as follows:

- (1) The frequency of the grid-connected current harmonics can be expressed as $(m\omega_c + n\omega_0)t$, i.e., the harmonics mainly occur around integer multiples of the equivalent carrier frequency
- (2) When n is an even number, there are no harmonics of an integer multiple of the equivalent carrier frequency in the grid-connected current
- (3) When the equivalent DC bus voltages of each phase are not equal, the harmonics of the grid-connected current will appear near the equivalent carrier frequency multiple, and the amplitude of the harmonic current is positively correlated with the difference of the equivalent DC bus voltages

- (4) In the same spectrum, the harmonic component of the grid-connected current decreases as the equivalent carrier frequency increases
- (5) The equivalent carrier frequency can be increased by increasing the number of microsources N or by increasing the carrier frequency f_c , thus reducing the harmonic content in the grid-connected current

Regarding the harmonic content of grid-connected current in a microgrid, the IEEE Std. 1547-2003 standard requires that the current THD should be less than 1.5% [29]. Therefore, to make the grid-connected current THD of the HCSY-MG system meet the requirement, the LCL filter parameter will be designed using the improved PSO-LSSVM algorithm in this study.

3. LCL Grid-Connected Filter Characteristics and Constraints

3.1. LCL Grid-Connected Filter Characteristics. The LCL grid-connected filter topology with a damping resistor is shown in Figure 4.

In Figure 4, u_i is the input voltage, i_o is the output grid-connected current, and u_o is the output voltage. Its open-loop transfer function can be obtained from Figure 4:

$$G(s) = \frac{R_f C_f s + 1}{L_c L_g C_f s^3 + (L_c + L_g) R_f C_f s^2 + (L_c + L_g) s}, \quad (10)$$

where s is the frequency domain variable.

Let $R_f = 0$ in the previous equation to obtain the open-loop transfer function of the LCL filter without the damping resistor. The Bode diagram of the LCL grid-connected filter is shown in Figure 5.

As can be seen from Figure 5, the LCL filter amplitude response curve without the damping resistor has a spike at the resonance point, while the phase response has a -180° change, which can easily lead to the instability of the grid-connected system and thus affect the safe and reliable operation of the power system. The damping resistor can cut the resonance spike in the amplitude response curve to a certain extent and avoid the -180° change in the phase response, i.e., avoid the instability of the grid-connected system and guarantee the safe and reliable operation of the power system.

3.2. LCL Grid-Connected Filter Constraints. The current flowing through the converter-side filter inductor L_c generates a ripple current on the operation of the switch device, which affects the effectiveness of the LCL filter. The ripple current Δi_{\max} can be expressed as

$$\Delta i_{\max} = \frac{u_i}{4 f_{\text{equ}} L_c}, \quad (11)$$

where f_{equ} is the equivalent carrier frequency.

The introduction of the damping resistor also brings some additional power losses. To ensure the filter performance, the power loss of the whole filter needs to be less than

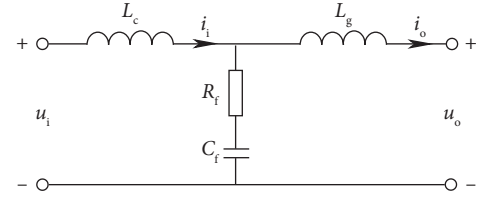


FIGURE 4: LCL grid-connected filter topology with a damping resistor.

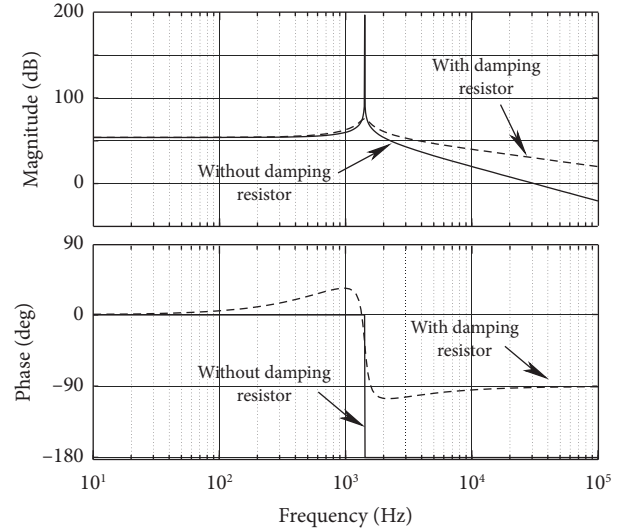


FIGURE 5: Bode diagram of the LCL grid-connected filter.

5% of the rated active power. The power loss of the filter can be given by [30]

$$P_{\text{loss}} = R_f \frac{u_o^2}{R_f^2 + 1/\omega_{\text{equ}}^2 C_f^2}, \quad (12)$$

where P_{loss} is the power loss of the filter and ω_{equ} is the equivalent carrier angular frequency.

The total inductance of the filter can effectively reduce the harmonic current content of the grid, but too large inductance will make the filter response to the current weak, so the total inductance of the filter needs to be reasonably selected. The constraint on the total filter inductance L can be given by [31]

$$\frac{u_i}{4\sqrt{3}\Delta i_{\max} \cdot f_{\text{equ}}} \leq L \leq \sqrt{\frac{u_{\max}^2 - u_i^2/3}{\omega_{\text{equ}}^2 i_{\max}^2}}, \quad (13)$$

where $L = L_c + L_g$, u_{\max} , and i_{\max} are the peak values of output voltage and current, respectively.

4. Improved PSO-LSSVM Algorithm

4.1. The PSO-LSSVM Algorithm. In the analysis of existing LCL filter parameter design methods and in the process of obtaining training samples, it was found that the attenuation of the harmonic amplitude of the grid-connected current by

the LC branch in the LCL filter is a nonlinear process. Also, because the number of training samples obtained by the simulation in this study is small and the LSSVM can obtain better results in the field of modeling and prediction of nonlinear data with a small sample size, LSSVM is used as the basic algorithm in this study. In addition, the use of the PSO algorithm to optimize the parameters affecting the anti-interference and generalization of LSSVM models has been widely used means. For these reasons, the PSO-LSSVM has good compatibility with the problem discussed in this study, so this algorithm is chosen as the core algorithm of this study.

Given a sample set $\{(x_j, y_j)\}$, $j = 1, 2, \dots, q$, where x_j is the input vector, y_j is the output vector, and q is the size of the sample set, then the optimization model of LSSVM can be given by [32]

$$\min [J(\omega, \xi)] = \frac{1}{2} \|\omega\|^2 + \frac{1}{2} P \sum_{j=1}^q \xi_j^2, \quad (14)$$

$$\text{s.t. } y_j = \omega \phi(x_j) + b + \xi_j, \quad j = 1, 2, \dots, q,$$

where ω is the weight vector, b is the bias, P is the error penalty factor, ξ_j is the relaxation variable, and $\phi(\cdot)$ is the nonlinear mapping function.

By solving the previous optimization model, the final regression model of LSSVM can be expressed as

$$f(x) = \sum_{j=1}^q \lambda_j K(x, x_j) + b, \quad (15)$$

where λ_j is the Lagrange multiplier and $K(x, x_j)$ is the kernel function.

To ensure the generalization of the regression model, the radial basis function is chosen as the kernel function, which can be expressed as

$$K(x, x_j) = \exp\left(-\frac{\|x - x_j\|^2}{2\sigma^2}\right), \quad (16)$$

where σ is the kernel parameter.

From the above standard type of LSSVM, it can be seen that the kernel parameter σ and the error penalty factor P will affect the anti-interference and generalization of the model, so they need to be optimized. Currently, the PSO algorithm is commonly used to optimize the previous two parameters of LSSVM, namely, the PSO-LSSVM model. The velocity and position of the particles in the PSO optimization algorithm are updated in the following way:

$$\begin{aligned} v_{t+1} &= \alpha v_t + \beta_1 \cdot \text{rand}(0, 1) (pbest_t - x_t) \\ &\quad + \beta_2 \cdot \text{rand}(0, 1) (gbest_t - x_t), \\ x_{t+1} &= x_t + v_t, \end{aligned} \quad (17)$$

where v_t is the speed of the particle, α is the inertia factor, β_1 is the self-learning factor, $\text{rand}(0, 1)$ is a random number between $(0, 1)$, $pbest_t$ is the current optimal position of the particle, x_t is the current position of the particle, β_2 is the

global-learning factor, and $gbest_t$ is the current global optimal position of the particle.

4.2. The Inertia Factor Adaptive Adjustment Strategy of Improved PSO-LSSVM. In this study, to balance the global-search and self-search capability of PSO-LSSVM while improving the model convergence speed, an inertia factor adaptive adjustment strategy has been used to make the inertia factor adjust its size according to the difference between two consecutive update directions. The inertia factor adaptive adjustment strategy can be expressed as

$$\alpha' = \begin{cases} D \cdot \alpha, & \Delta v > 0, \\ d \cdot \alpha, & \Delta v < 0, \end{cases} \quad (18)$$

where α' is the inertia factor after updating, D is the rate of inertia increase, and d is the rate of inertia decrease.

PSO-LSSVM is already a mature model in which the PSO algorithm is widely used and can achieve the global optimality. In addition, the adaptive adjustment of inertia can give the improved PSO-LSSVM model the ability to flush out the current optimal value and find the global optimal value. Therefore, the proposed improved PSO-LSSVM in this study can reach the global optimum.

In summary, when the maximum number of iterations is maxgen, the flowchart of the PSO-LSSVM algorithm for adaptive inertia is shown in Figure 6.

5. Parameter Design of the LCL Grid-Connected Filter Based on Improved PSO-LSSVM

The steps for the design of LCL grid-connected filter parameters based on the improved PSO-LSSVM are as follows:

- (1) Based on the constraint related to the ripple current, the design value of the converter-side filter inductor is found
- (2) According to the improved PSO-LSSVM, the design values of the filter capacitor and grid-side filter inductor are obtained
- (3) According to the power loss constraints of the LCL filter, the design value of the damping resistor is found
- (4) The other constraints are checked for the designed LCL filter
- (5) If the constraint is satisfied, the designed LCL filter is the desired one; if the constraint is not satisfied, we return to step (1) and redesign

5.1. Converter-Side Filter Inductor Design. The characteristics of the LCL filter show that the ripple current flowing through the filter inductor on the converter-side affects the performance of the filter. The expression of the ripple current is shown in (11), which contains the relevant parameter for the converter-side filter inductor. Then, the converter-side filter inductor can be expressed as

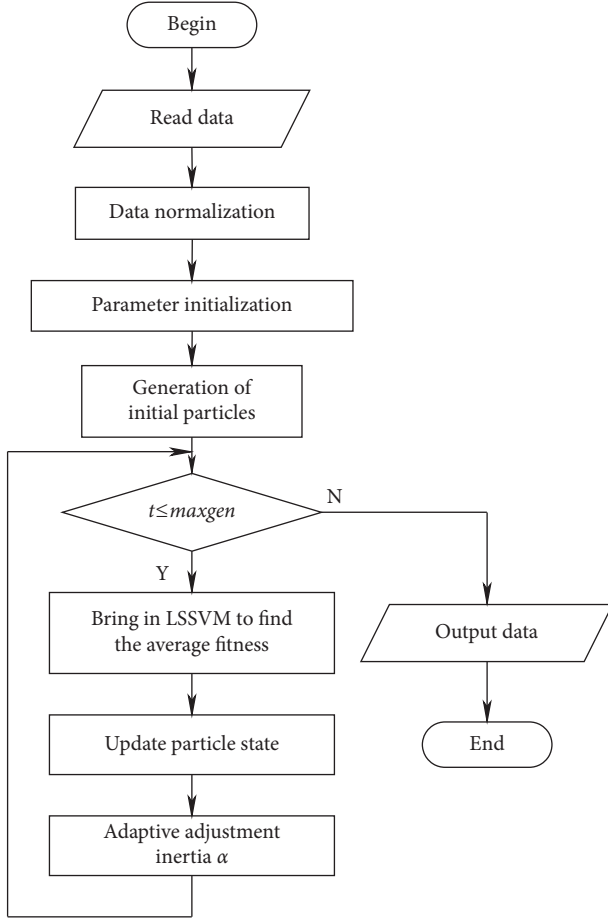


FIGURE 6: Flowchart of the PSO-LSSVM algorithm for adaptive inertia.

$$L_c = \frac{u_i}{4f_{\text{equ}}\Delta i_{\text{max}}}. \quad (19)$$

Let the equivalent DC chain voltage $u_{\text{dci}} = 80\text{V}$, microsource number $N=4$, and the carrier frequency $f_c = 1\text{kHz}$ of the HCSY-MG system. Then, according to (19), the converter-side filter inductance can be calculated as $L_c = 1\text{mH}$, so the design value of L_c is chosen as 1mH .

5.2. Parameter Design Based on Improved PSO-LSSVM

5.2.1. Determination of Model Input and Output Vectors. Combining the analysis of the LCL grid-connected filter characteristics in Section 3 and the analysis of harmonic characteristics of the grid-connected current of the HCSY-MG system in Section 2.2, the input vectors of the filter parameter design model based on improved PSO-LSSVM are chosen as the equivalent DC chain voltage, converter output voltage, equivalent carrier frequency, high-frequency harmonic current content (including $f_{\text{equ}} - 5f_n$, $f_{\text{equ}} - 3f_n$, $f_{\text{equ}} - f_n$, $f_{\text{equ}} + f_n$, $f_{\text{equ}} + 3f_n$, and $f_{\text{equ}} + 5f_n$), current THD allowable value, and desired resonant frequency, in 11 groups. The output vectors are selected as the grid-side filter inductor value and filter capacitor value, in 2 groups. Here, f_{equ} and f_n are the

equivalent carrier frequency and fundamental frequency, respectively.

5.2.2. Data Preprocessing and Model Evaluation Metrics. From the correlation analysis in Section 3, it is clear that the variables in the input and output vectors have large order-of-magnitude differences. To ensure the accuracy of model building and the homogeneity of the data, the data need to be normalized using a linear transformation.

To measure the effectiveness of the improved PSO-LSSVM algorithm and the feasibility and effectiveness of the filter parameter design method based on the improved PSO-LSSVM, the fitness function is selected as

$$g = \frac{1}{2}(f(x_i) - y_i)^2. \quad (20)$$

In addition, the root mean square error (RMSE) and the mean relative error (MRE) were selected as the network evaluation criteria.

5.2.3. Validation of Improved Strategies. Based on the designed converter-side filter inductor, the feasibility and effectiveness of the improved PSO-LSSVM are verified by obtaining training sample sets through simulation.

According to the description related to the improved PSO-LSSVM model in Section 4, the basic parameters are selected as the self-learning factor $\beta_1 = 1.5$ and the global-learning factor $\beta_2 = 1.7$, and the maximum number of iterations is set to 60.

The effectiveness of the proposed improved PSO-LSSVM model in improving the convergence speed is first verified by comparison. Under the same model parameters and training sample set, the PSO-LSSVM fitness function curves using the inertia factor adaptive adjustment strategy and the common strategy are shown in Figure 7. The corresponding network evaluation metrics are shown in Table 1.

From the change curve of the fitness function in Figure 7, it can be seen that when the inertia factor in the particle velocity update formula adopts an adaptive adjustment strategy, the value of the fitness function can be stabilized at a smaller value sooner and the convergence of the model can be accelerated, which in turn ensures the applicability of the model in the case of a small training sample set.

As can be seen from the data in Table 1, when the inertia factor is adjusted with the adaptive adjustment strategy, it does not have a large impact on the error of the model, but it can slightly improve the accuracy of the model. In addition, since the adaptive inertia factor adjustment strategy adjusts the inertia of the particle velocity update after each iteration, there is a certain extension of the model training time.

5.2.4. Filter Capacitor and Grid-Side Filter Inductor Design. Based on the previous improved PSO-LSSVM model, the input vectors are set as shown in Table 2.

Then, the corresponding output vectors are obtained by the improved PSO-LSSVM as shown in Table 3.

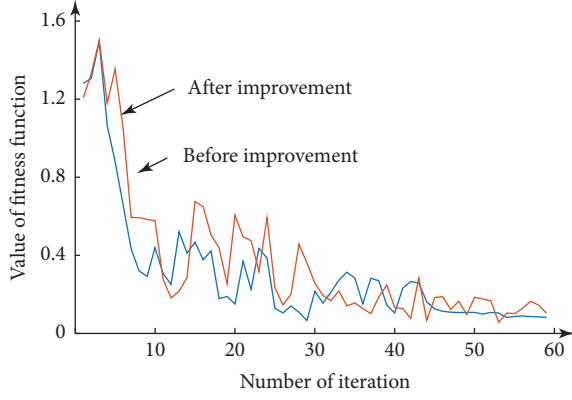


FIGURE 7: PSO-LSSVM adaptation function curves before and after improvement.

TABLE 1: PSO-LSSVM network evaluation metrics before and after improvement.

| Models | RMSE | MRE (%) | Training time (s) |
|-----------------------|--------|---------|-------------------|
| PSO-LSSVM | 0.1725 | 5.9145 | 3.81 |
| Improvement PSO-LSSVM | 0.1703 | 5.8169 | 4.27 |

TABLE 2: Improved PSO-LSSVM model input vector.

| Numbers | Input vector name | Input vector value |
|---------|--|--------------------|
| 1 | Equivalent DC chain voltage | 320 V |
| 2 | Converter output voltage | 160 V |
| 3 | Equivalent carrier frequency | 4 kHz |
| 4 | $f_{\text{equ}} - 5f_n$ harmonic content | 1% |
| 5 | $f_{\text{equ}} - 3f_n$ harmonic content | 0.5% |
| 6 | $f_{\text{equ}} - f_n$ harmonic content | 1% |
| 7 | $f_{\text{equ}} + f_n$ harmonic content | 1% |
| 8 | $f_{\text{equ}} + 3f_n$ harmonic content | 0.5% |
| 9 | $f_{\text{equ}} + 5f_n$ harmonic content | 1% |
| 10 | THD of current | 1.5% |
| 11 | Desired resonant frequency | 3 kHz |

TABLE 3: Improved PSO-LSSVM model output vector.

| Numbers | Output vector name | Output vector value |
|---------|---------------------------------|----------------------|
| 1 | Grid-side filter inductor value | 0.124 mH |
| 2 | Filter capacitor value | 18.426 μF |

Considering the actual component values, the design value of the grid-side filter inductor designed value is 0.1 mH and the capacitor designed value is 20 μF .

5.3. Design of the Damping Resistor. The designed value of the damping resistor can be obtained from Subsection 3.2 by the filter power loss, i.e., equation (12). Let the $P_{\text{loss}} = 5\%P$, then the value of the damping resistor is calculated to be $R_f = 0.48\Omega$. Therefore, the design value of the damping resistor is chosen as 0.5 Ω .

The verification of whether the designed LCL filter satisfies the relevant constraints will be performed later.

6. Simulation Verification

Based on the abovementioned method, a grid-connected simulation model is built based on the obtained HCSY-MG system parameters and the parameters of each element of the LCL grid-connected filter, to validate the results and conclusions drawn.

6.1. Verification of Grid-Connected Current Characteristics. First, the grid-connected current characteristics of the HCSY-MG system are verified. The grid-connected current waveform and its spectrum when the LCL filter is not added to the HCSY-MG grid-connected system are shown in Figure 8.

From Figure 8(a), it can be seen that the grid-connected current has some sinusoidal characteristics, but the overall quality is poor. Figure 8(b) can reflect the following characteristics: (i) the grid-connected current does not contain harmonics at an integer multiple of the equivalent carrier frequency; (ii) the harmonic currents are mainly distributed near the equivalent carrier frequency multiple; (iii) the harmonic content decreases with the increase of the equivalent carrier frequency. This proves the correctness of the analysis of the harmonic characteristics of the grid-connected current of the HCSY-MG system in Section 2.2. In addition, the grid-connected current THD = 13.11%, which is greater than the 1.5% required by IEEE Std. 1547-2003 standard, so it cannot be directly connected to the grid.

6.2. LCL Filter Performance Verification. Then, the feasibility of the proposed filter parameter design method based on improved PSO-LSSVM is verified.

We set the LCL grid-connected filter with each element parameter as described in Section 5.2, i.e., $L_c = 1\text{mH}$, $L_g = 0.1\text{mH}$, $C_f = 20\mu\text{F}$, and $R_f = 0.5\Omega$, to obtain the corresponding filter transfer function as

$$G(s) = \frac{R_f C_f s + 1}{L_c L_g C_f s^3 + (L_c + L_g) R_f C_f s^2 + (L_c + L_g) s} \quad (21)$$

$$= \frac{10 \times 10^{-6} s + 1}{2 \times 10^{-12} s^3 + 11 \times 10^{-9} s^2 + 1.1 \times 10^{-3} s}.$$

The Bode diagram corresponding to the transfer function $G(s)$ is shown in Figure 9.

From the LCL filter Bode plot magnitude response curve in Figure 9, it can be seen that the LCL filter designed based on the improved PSO-LSSVM algorithm can effectively suppress high-frequency harmonics. From the phase response curve, it can be seen that the designed filter has a phase change of -135° at the resonant frequency and does not have a change of -180° which can easily lead to system instability, so the design of each element parameter of the filter is reasonable and does not make the grid-connected system unstable.

The LCL filter was connected to the HCSY-MG grid-connected system, and the waveforms of the grid-connected current and its spectrum are obtained as shown in Figure 10.

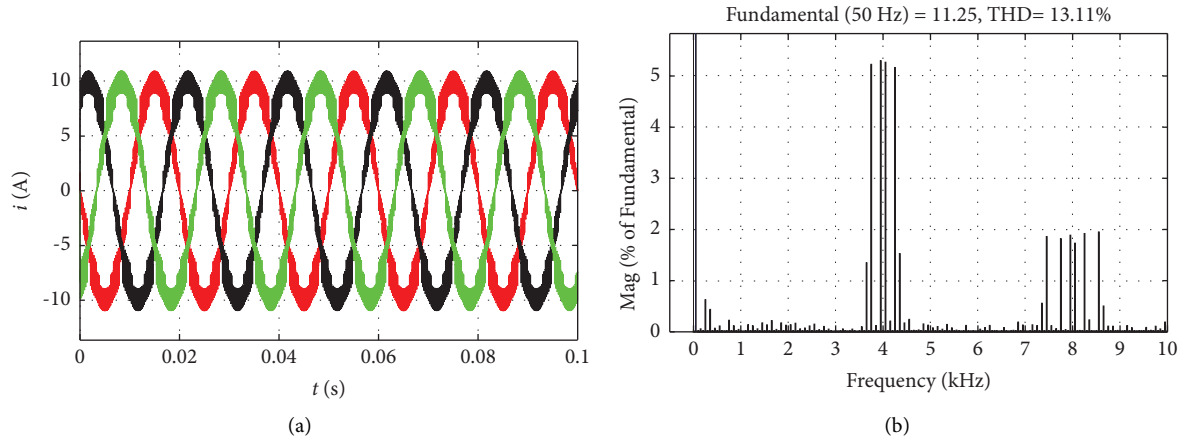


FIGURE 8: Waveform of the grid-connected current without a filter and its frequency spectrum. (a) Waveform of the grid-connected current and (b) frequency spectrum of the grid-connected current.

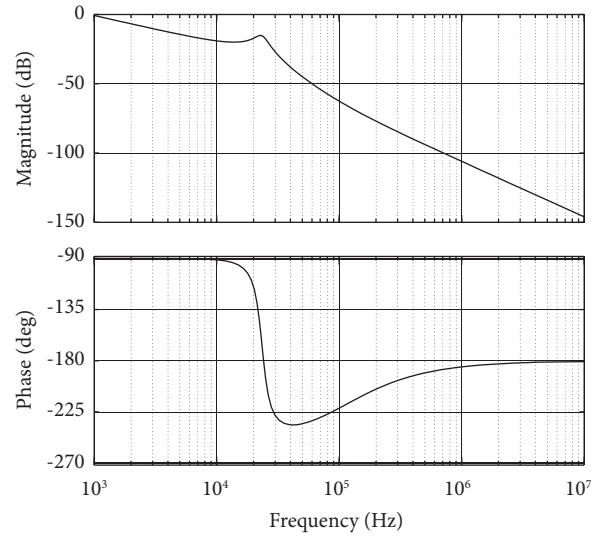


FIGURE 9: LCL filter diagram after parameter design.

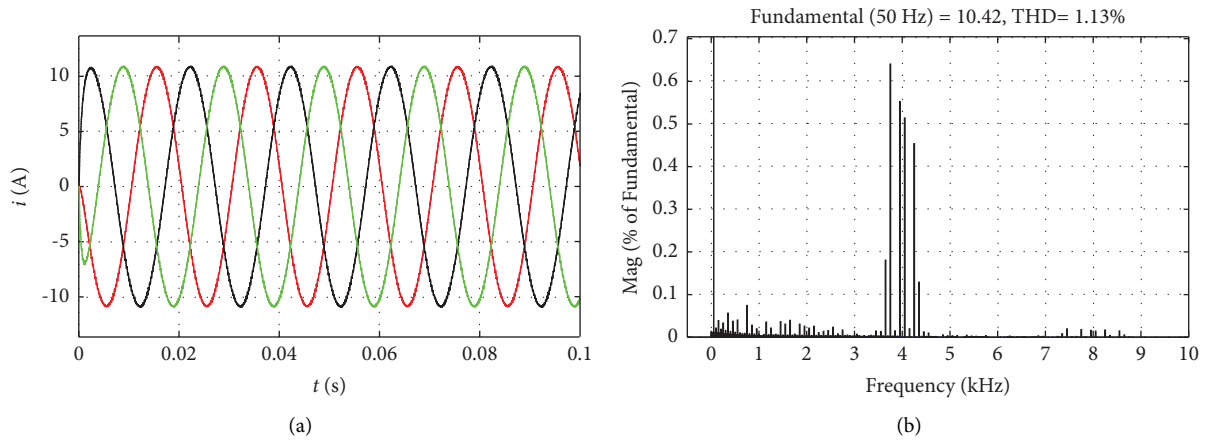


FIGURE 10: The waveform of the grid-connected current with a filter and its spectrum. (a) Waveform of the grid-connected current and (b) frequency spectrum of the grid-connected current.

TABLE 4: The LCL filter parameter designed by different methods and the corresponding parameter HCSY-MG system grid-connected current.

| | L_c (mH) | L_g (mH) | C_f (μ F) | Fundamental | THD (%) | f_r (Hz) |
|--|------------|------------|------------------|-------------|---------|------------|
| Design method in this paper | 1 | 0.1 | 20 | 10.42 | 1.13 | 3734 |
| Traditional design method | 1 | 0.5 | 10 | 10.4 | 1.7 | 2758 |
| Graphical analysis method | 1 | 0.4 | 6 | 10.42 | 1.75 | 3845 |
| Optimized parameter method | 1 | 0.5 | 5 | 10.4 | 1.83 | 3900 |
| Multivariate system of equation method | 1.2 | 0.6 | 10 | 9.8 | 1.38 | 2517 |

From Figure 10(a), it can be seen that the power quality of the grid-connected current is better. Figure 10(b) shows that the current THD is reduced to 1.13%, which meets the conditions required in IEEE Std. 1547-2003 standard, the harmonic current content near 4 kHz is less than 1%, and the harmonic current content near 8 kHz is extremely low, reaching a negligible level. Therefore, by comparing Figures 8 and 10, it can be seen that the LCL filter designed based on the method proposed in this study can effectively improve the power quality of the grid-connected current and reduce the harmonic content in the grid-connected current.

6.3. LCL Filter Constraint Verification. According to the design steps in Section 5, it is necessary to verify whether the designed LCL filter satisfies the corresponding constraints. In addition to the constraints already verified in the previous section, the remaining conditions are to be verified as follows.

6.3.1. Resonant Frequency. According to the design of each element parameter of the LCL filter in Section 5, the corresponding resonant frequency of the filter can be calculated as

$$f_{\text{res}} = \frac{1}{2\pi} \sqrt{\frac{L_c + L_g}{L_c L_g C_f}} = 3734 \text{ Hz}. \quad (22)$$

For the resonant frequency f_{res} , the general constraint can be expressed as

$$10f_0 \leq f_{\text{res}} \leq f_{\text{equ}}. \quad (23)$$

Comparing equations (22) and (23), it is found that the designed filter satisfies the constraint of the resonant frequency.

6.3.2. Total Inductance. According to the constraint of (13) for the total inductance value, it can be calculated as $0.58 \text{ mH} \leq L = 1.1 \text{ mH} \leq 346 \text{ mH}$. Therefore, the total inductance value $L = 1.1 \text{ mH}$ satisfies the relevant constraint.

Simulation and verification results show that the LCL grid-connected filter design method based on the improved PSO-LSSVM algorithm proposed in this study can effectively reduce the harmonic content in the grid-connected current without destabilizing the HCSY-MG grid-connected system and meet the corresponding constraint requirements.

6.4. LCL Filter Contrast Analysis. To illustrate the advantages of the proposed LCL grid-connected filter parameter design method for the HCSY-MG system over the existing methods

and its applicability to the HCSY-MG system, the comparative analysis of the previous methods is necessary. The LCL filter parameters designed by different methods and the corresponding parameters of the HCSY-MG system grid-connected current are shown in Table 4, where the target of optimized parameter method is the minimization of energy storage element values of the literature [19].

Compared with the traditional design method, the design method proposed in this study does not need to rely on the iterative trial of engineering experience. Compared with the graphical analysis method, the design method proposed in this study also avoids iterative trial and does not require a complicated graphing process to obtain the desired filter parameters. The optimized parameter method can only consider one or more objectives and cannot comprehensively consider the requirements of the whole system, while the method proposed in this study can measure the characteristics of the whole system comprehensively with the help of the machine learning model, i.e., the improved PSO-LSSVM, and thus derive more reasonable filter parameters. Although the multivariate system of the equations' method represents the system characteristics by a system of equations, the resulting system of equations is difficult to solve, while the method proposed in this study only requires the data obtained from the HCSY-MG system operation to design reasonable filter parameters easily.

Comparing the design results, it can be seen that the total inductance of the LCL filter designed based on the method proposed in this study is the smallest, and the grid-connected current THD is also smaller; although the filter capacitance is larger, it still meets the corresponding constraint requirements. In addition, the method proposed in this study is more applicable to the HCSY-MG system, and also, the input and output vector of the improved PSO-LSSVM can be flexibly adjusted according to the actual application objects.

6.5. Sensitivity Analysis. When the parameters of the HCSY-MG system change, the power quality parameters of its grid-connected current will also change. The LCL filter parameter design method for the HCSY-MG system used in this study uses the grid-connected current characteristics of the HCSY-MG system as the training samples for the improved PSO-LSSVM model, and even the parameters of the HCSY-MG system change, the corresponding training samples will also change. Therefore, when the parameters of the HCSY-MG system change, with the modeling and prediction capability of the improved PSO-LSSVM model, the results of the LCL grid-connected filter parameters

TABLE 5: Sensitivity analysis of different D and d .

| D, d | 1.1, 0.4 | 1.1, 0.6 | 1.1, 0.8 | 1.5, 0.4 | 1.5, 0.6 | 1.5, 0.8 | 1.7, 0.4 | 1.7, 0.6 | 1.7, 0.8 |
|------------------------------|---------------|----------------|----------------|----------------|----------------|----------------|----------------|----------------|----------------|
| Training time (s) | 4.31 | 4.28 | 4.18 | 4.24 | 4.27 | 4.26 | 4.32 | 4.27 | 4.30 |
| RMSE, MRE | 0.1965, 6.376 | 0.1786, 5.9287 | 0.4106, 6.5487 | 0.1891, 6.1412 | 0.1703, 5.8169 | 0.2013, 6.2148 | 0.5162, 7.1047 | 0.1862, 6.1064 | 0.1807, 6.2303 |
| L_g (mH), C_f (μ F) | 0.102, 20.208 | 0.146, 17.712 | 0.217, 14.784 | 0.145, 19.481 | 0.124, 18.426 | 0.134, 19.386 | 0.267, 21.420 | 0.162, 20.714 | 0.126, 18.711 |
| Fund., THD | 10.42, 1.13% | 10.15, 1.05% | 10.06, 1.12% | 10.13, 1.05% | 10.42, 1.13% | 10.13, 1.05% | 10.52, 2.11% | 10.27, 1.07% | 10.42, 1.13% |

designed based on the method proposed in this study will also be designed in accordance with the system requirements.

The improved PSO-LSSVM used in the LCL filter parameters design method proposed in this study consists of three core components, which are the PSO optimization algorithm, the LSSVM model, and the inertia factor adaptive algorithm. Among them, the inertia factor adaptive algorithm is an innovation in this study. Many analyses of the sensitivity of the parameters of the PSO optimization algorithm have been made in the existing literature, as well as a sensitivity analysis of the LSSVM model has been given in the literature [32]. So, a corresponding sensitivity analysis of the inertia factor adaptive algorithm will be given as follows.

The description of increasing rate D and decreasing rate d in Subsection 4.2 shows that these two parameters only affect the convergence speed of the improved PSO-LSSVM when they are varied within a reasonable range of values and do not have a large impact on the design results and training time. To verify this conjecture, the improved PSO-LSSVM network evaluation metrics and training time, the corresponding filter design values, and the HCSY-MG grid-connected current power quality parameters for different values of D and d are summarized in Table 5. The results for the fundamental component and THD are obtained according to the inductance and capacitance values that match the actual situation.

As can be seen from the table, too large or too small rates may cause large errors in the improved PSO-LSSVM modeling and prediction results, but they do not have a large impact on the training time. The previous validation results are the same as the theoretical analysis. The reason that too large or too small rates make the improved PSO-LSSVM modeling and prediction results to have large errors may be the inability to converge to the global optimal solution with a finite number of iterations constraint. When the global optimal solution cannot be obtained by the improved PSO-LSSVM, it will make the designed LCL filter fail to meet the requirements of the HCSY-MG grid-connected operation. Therefore, the values of D and d chosen in this study are the values for the minimum case of RMSE and MRE, i.e., $D = 1.5$ and $d = 0.6$.

7. Conclusion

The LCL grid-connected filter parameter design method proposed in this study is firstly for a new type of series microgrid which is the HCSY-MG system. Then, a new method is proposed to design the HCSY-MG grid-connected filter parameters using the improved PSO-LSSVM, in which the power quality of the grid-connected current is used as the input vector of the improved PSO-LSSVM, and the parameters of the LC in the filter are taken as the output vector to obtain the LCL filter parameters that meet the design requirements according to the HCSY-MG system operating characteristics and relevant constraints.

The main work and innovations of this study are as follows: (1) Based on the HCSY-MG mathematical model of grid-connected operation, the characteristics of the grid-

connected current of the system are analyzed and obtained. (2) Combining with the application context, an improved PSO-LSSVM is proposed by adaptively adjusting the size of the inertia factor by (18) according to the direction of the two consecutive particle velocity in the PSO-LSSVM. (3) Based on the previous research work, a parameter design method of the LCL grid-connected filter for the HCSY-MG system based on the improved PSO-LSSVM is proposed.

The positive points of the proposed work are as follows: (1) The grid-connected current characteristics of the HCSY-MG system, a new type of series microgrid, are analyzed to provide a reference for the subsequent grid-connected operation and control of the system. (2) The LCL grid-connected filter parameter design method based on the improved PSO-LSSVM is proposed for the HCSY-MG system, which reduces the THD of grid-connected current from 13.11% to 1.13% and effectively improves the power quality of the grid-connected current of the HCSY-MG system. The proposed method provides a new idea and method for the design of grid-connected filter parameters of microgrids. (3) For the application context of this study, an improved PSO-LSSVM with adaptive change of the inertia factor is proposed, which improves the convergence speed of the model and enriches the application of PSO-LSSVM.

Data Availability

The data used to support the findings of this study are available from the corresponding author upon request.

Conflicts of Interest

The authors declare that they have no conflicts of interest.

Acknowledgments

This research was funded by the National Natural Science Foundation of China (grant no. 51967011).

References

- [1] M. Begovi, A. Pregelj, A. Rohatgi, and D. Novosel, "Impact of renewable distributed generation on power systems," in *Proceedings of the 34th Hawaii International Conference on System Sciences*, pp. 654–663, Baden, Switzerland, June 2001.
- [2] C. Wang, Z. Wu, and P. Li, "Research on key technologies of microgrid," *Transactions of China Electrotechnical Society*, vol. 29, no. 2, pp. 1–12, 2014.
- [3] X. Yang, J. Su, Z. Lv, and Y. Zhao, "Overview on micro-grid technology," *Proceedings of the CSEE*, vol. 34, no. 1, pp. 57–70, 2014.
- [4] W. Feng, K. Sun, Y. Guan, and M. G. Josep, "A harmonic current suppression strategy for voltage source grid-connected inverters based on output voltage hybrid control in islanded microgrids," *Transactions of China Electrotechnical Society*, vol. 31, no. 7, pp. 72–80, 2016.
- [5] C. Tu, Y. Yang, F. Xiao, and Z. Lan, "The output side power quality control strategy for microgrid main inverter under nonlinear load," *Transactions of China Electrotechnical Society*, vol. 33, no. 11, pp. 2486–2495, 2018.

- [6] X. Wang and W. Yang, "Study on characteristics of a microgrid with micro source inverters connected in series," *Power System Protection and Control*, vol. 41, no. 21, pp. 129–135, 2013.
- [7] X. Wang, S. Xue, and X. Li, "Analysis of output characteristics of a microgrid based on modular Multilevel converter half-bridge series structure," *Transactions of China Electrotechnical Society*, vol. 34, no. 10, pp. 2130–2140, 2019.
- [8] N. Khosravi, A. Abdolvand, A. Oubelaid, Y. A. Khan, M. Bajaj, and S. Govender, "Improvement of power quality parameters using modulated-unified power quality conditioner and switched-inductor boost converter by the optimization techniques for a hybrid AC/DC microgrid," *Scientific Reports*, vol. 12, no. 1, Article ID 21675, 2022.
- [9] S. Koganti, K. J. Koganti, and S. R. Salkuti, "Design of multi-objective-based artificial intelligence controller for wind/battery-connected Shunt active power filter," *Algorithms*, vol. 15, no. 8, pp. 256–323, 2022.
- [10] N. Khosravi, H. R. Abdolmohammadi, S. Bagheri, and M. R. Miveh, "A novel control approach for harmonic compensation using switched power filter compensators in Micro-grids," *IET Renewable Power Generation*, vol. 15, no. 16, pp. 3989–4005, 2021.
- [11] M. Liserre, F. Blaabjerg, and S. Hansen, "Design and control of an LCL-filter based three-phase active rectifier," *IEEE Transactions on Industry Applications*, vol. 41, no. 5, pp. 1281–1291, 2005.
- [12] Q. Liu, L. Peng, S. Tang, and S. Yang, "Design and optimization method of LCL filters based on the graphic-analysis," *Proceedings of the CSEE*, vol. 32, no. 36, pp. 36–43, 2012.
- [13] X. Jiang, C. He, and B. Tang, "Optimization and design of parameters for LCL filter of on-grid inverter," *Acta Energaie Solaris Sinica*, vol. 37, no. 10, pp. 2533–2538, 2016.
- [14] X. Chen, F. Lu, M. Ding, and X. Wu, "A new design of LCL filter for three-phase voltage-source PWM rectifier," *Journal of North China Electric Power University*, vol. 38, no. 5, pp. 110–116, 2011.
- [15] K. Jalili and S. Bernet, "Design of LCL filters of active-front-end two-level voltage-source converters," *IEEE Transactions on Industrial Electronics*, vol. 56, no. 5, pp. 1674–1689, 2009.
- [16] Y. Wang, F. Wu, L. Sun, and F. Chen, "Optimized design of LCL filter for minimal damping power loss," *Proceedings of the CSEE*, vol. 30, no. 27, pp. 90–95, 2010.
- [17] F. Liu, X. Zha, and S. Duan, "Design and research on parameter for LCL filter in three-phase grid-connected inverter," *Transactions of China Electrotechnical Society*, vol. 25, no. 3, pp. 110–116, 2010.
- [18] Y. J. Kim and H. Kim, "Optimal design of LCL filter in grid-connected inverters," *IET Power Electronics*, vol. 12, no. 7, pp. 1774–1782, 2019.
- [19] J. Wu, X. Ma, R. Hou, and D. Guangren, "Optimization of APF LCL output filter based on genetic algorithm," *Transactions of China Electrotechnical Society*, vol. 26, no. 5, pp. 159–164+177, 2011.
- [20] Y. Huang, Y. Tang, M. Yu, and J. Liu, "Parameter optimization design of grid-connected inverter LCL filter," *Electrical Measurement & Instrumentation*, vol. 56, no. 12, pp. 85–89, 2019.
- [21] Y. Yuan and C. Liu, "Passive power filter optimization problem based on adaptive multipopulation NSGA-II and CRITIC-TOPSIS," *Mathematical Problems in Engineering*, vol. 2022, Article ID 5753651, 18 pages, 2022.
- [22] X. Zheng, L. Xiao, and B. Wang, "A new parameter optimization method of LCL filters in three-phase converters," *Proceedings of the CSEE*, vol. 33, no. 12, pp. 55–63, 2013.
- [23] L. Kong, W. Wang, and H. Wang, "Parameter optimization design method of LCL filter for photovoltaic grid-connected inverter," *Computer Simulation*, vol. 38, no. 8, pp. 75–80, 2021.
- [24] Y. X. Cai, Y. J. He, H. W. Zhou, and J. Liu, "Design method of LCL filter for grid-connected inverter based on particle swarm optimization and screening method," *IEEE Transactions on Power Electronics*, vol. 36, no. 9, pp. 10097–10113, 2021.
- [25] H. Yang, F. Tian, P. Zhang, and W. Yongjun, "Short-term load forecasting based on CEEMD-FE-AOA-LSSVM," *Power System Protection and Control*, vol. 50, no. 13, pp. 127–133, 2022.
- [26] X. Yang, Z. Zhao, Y. Yang, and V. Miranda, "Research on distributed photovoltaic power prediction method based on combination of spatiotemporal information," *Thermal Power Generation*, vol. 51, no. 8, pp. 64–72, 2022.
- [27] J. Lin and S. Wang, "Research on fault diagnosis of jointless track circuit based on DBN-MPA-LSSVM," *Journal of Electronic Measurement and Instrument*, vol. 10, pp. 1–8, 2022.
- [28] B. Li, R. Yang, D. Xu, G. Wang, W. Wang, and D. Xu, "Analysis of the phase-shifted carrier modulation for modular Multilevel converters," *IEEE Transactions on Power Electronics*, vol. 30, no. 1, pp. 297–310, 2015.
- [29] IEEE, "IEEE Standard for Interconnecting Distributed Resources with Electric Power Systems," *IEEE Std*, vol. 1547, 2003.
- [30] Q. Zhong, J. Tong, X. Ma, and G. Wang, "Deterministic design of LCL filter for voltage source converter," *High Voltage Engineering*, vol. 42, no. 10, pp. 3068–3074, 2016.
- [31] X. Zheng, M. Li, Y. Wang, and F. Zare, "A novel parameter optimization strategy for LCL filters for grid-tied inverters," *Electronic Measurement Technology*, vol. 45, no. 8, pp. 14–20, 2022.
- [32] J. A. K. Suykens and J. Vandewalle, "Least Squares support vector machine classifiers," *Neural Processing Letters*, vol. 9, no. 3, pp. 293–300, 1999.



控制理论与应用
Control Theory & Applications
ISSN 1000-8152, CN 44-1240/TP

《控制理论与应用》网络首发论文

题目：基于波动量自适应补偿的 HCSY-MG 系统并网电流模型预测控制
作者：李锦键，王兴贵，李昱，丁颖杰，薛晟
收稿日期：2024-07-19
网络首发日期：2025-04-09
引用格式：李锦键，王兴贵，李昱，丁颖杰，薛晟. 基于波动量自适应补偿的 HCSY-MG 系统并网电流模型预测控制[J/OL]. 控制理论与应用.
<https://link.cnki.net/urlid/44.1240.TP.20250408.1903.008>



网络首发：在编辑部工作流程中，稿件从录用到出版要经历录用定稿、排版定稿、整期汇编定稿等阶段。录用定稿指内容已经确定，且通过同行评议、主编终审同意刊用的稿件。排版定稿指录用定稿按照期刊特定版式（包括网络呈现版式）排版后的稿件，可暂不确定出版年、卷、期和页码。整期汇编定稿指出版年、卷、期、页码均已确定的印刷或数字出版的整期汇编稿件。录用定稿网络首发稿件内容必须符合《出版管理条例》和《期刊出版管理规定》的有关规定；学术研究成果具有创新性、科学性和先进性，符合编辑部对刊文的录用要求，不存在学术不端行为及其他侵权行为；稿件内容应基本符合国家有关书刊编辑、出版的技术标准，正确使用和统一规范语言文字、符号、数字、外文字母、法定计量单位及地图标注等。为确保录用定稿网络首发的严肃性，录用定稿一经发布，不得修改论文题目、作者、机构名称和学术内容，只可基于编辑规范进行少量文字的修改。

出版确认：纸质期刊编辑部通过与《中国学术期刊（光盘版）》电子杂志社有限公司签约，在《中国学术期刊（网络版）》出版传播平台上创办与纸质期刊内容一致的网络版，以单篇或整期出版形式，在印刷出版之前刊发论文的录用定稿、排版定稿、整期汇编定稿。因为《中国学术期刊（网络版）》是国家新闻出版广电总局批准的网络连续型出版物（ISSN 2096-4188，CN 11-6037/Z），所以签约期刊的网络版上网络首发论文视为正式出版。

基于波动量自适应补偿的HCSY-MG系统并网电流模型预测控制

李锦键¹, 王兴贵^{1†}, 李 昱¹, 丁颖杰¹, 薛 晟^{1,2}

(1. 兰州理工大学 电气工程与信息工程学院, 甘肃 兰州 730050; 2. 甘肃省工业过程先进控制重点实验室, 甘肃 兰州 730050)

摘要: 在半桥变流器串联结构星型连接微电网(half-bridge converter series Y-connection microgrids, HCSY-MG)并网系统中, 可再生能源功率的波动将会引起并网电流中出现直流和基频波动量. 为解决以上HCSY-MG系统存在的特殊问题, 有针对性地提出一种基于波动量自适应补偿的并网电流模型预测控制策略. 在可再生能源存在随机波动的情况下, 得到HCSY-MG 系统的并网电流表达式, 并对其特性进行分析. 从上述特性出发, 将并网电流表达式作为预测模型, 并使用混沌化和自适应思想对青蒿素优化算法进行改进, 提高滚动优化环节的寻优速度, 同时降低并网电流中包含的波动量, 提高控制效果与精度. 最后与现有方法进行仿真和实验对比, 验证了本文所提控制策略的可行性、有效性和针对性.

关键词: 微电网; 模型预测控制; 并网电流; 波动量补偿; 改进青蒿素优化

引用格式: 李锦键, 王兴贵, 李昱, 等. 基于波动量自适应补偿的HCSY-MG系统并网电流模型预测控制. 控制理论与应用

DOI: 10.7641/CTA.2025.40380

Model predictive control of grid-connected current in HCSY-MG system based on adaptive compensation of fluctuating quantities

LI Jin-jian¹, WANG Xing-gui^{1†}, LI Yu¹, DING Ying-jie¹, XUE Sheng^{1,2}

(1. School of Electrical Engineering and Information Engineering, Lanzhou University of Technology, Lanzhou Gansu 730050, China;
2. Key Laboratory of Gansu Advanced Control for Industrial Processes, Lanzhou Gansu 730050, China)

Abstract: In the grid-connected system of a half-bridge converter series Y-connection microgrid (HCSY-MG), fluctuations in renewable energy power will introduce DC and fundamental frequency fluctuation components in the grid-connected current. To address this specific issue in the HCSY-MG system, a grid-connected current model predictive control strategy based on adaptive compensation of fluctuation components is proposed. Under the condition of stochastic fluctuations in renewable energy, the grid-connected current expression of the HCSY-MG system is derived, and its characteristics are analyzed. Based on these characteristics, the grid-connected current expression is utilized as the predictive model, and the artemisinin optimization algorithm is improved using chaotic and adaptive mechanisms to enhance the search speed in the rolling optimization process. This approach effectively reduces the fluctuation components in the grid-connected current while improving control performance and accuracy. Finally, simulations and experimental comparisons with existing methods verify the feasibility, effectiveness, and specificity of the proposed control strategy.

Key words: microgrids; model predictive control; grid-connected current; volatility compensation; improved artemisinin optimization algorithm

Citation: LI Jinjian, WANG Xinggui, LI Yu, et al. Model predictive control of grid-connected current in HCSY-MG system based on adaptive compensation of fluctuating quantities. *Control Theory & Applications*

1 引言

以光伏和风电为主的可再生能源发电不仅可以缓解一次能源紧缺的资源现状, 而且能够降低对环境的污染. 为充分利用可再生能源发电的技术、经

济、环境优势, 微电网的概念在2001年由美国电力可靠性技术协会提出^[1]. 微电网是一种将多个微源与负荷组合, 并且能为本地负荷提供电能的可控微型电力系统^[2]. 微电网经过多年的发展, 其中的交流微电网

收稿日期: 2024-07-19; 录用日期: 2025-02-10.

[†]通信作者. E-mail: Wangxg8201@163.com; Tel.: +86 0931-2973506.

本文责任编辑: 李德伟

国家自然科学基金项目(51967011), 甘肃省科技计划项目(联合科研基金重点项目)(24JRRA1205), 甘肃省杰出青年基金项目(22JR5RA221) 资助.

Supported by the National Natural Science Foundation of China (51967011), Gansu Provincial Science and Technology Project (Joint Research Fund Key Project) (24JRRA1205) and Gansu Outstanding Youth Foundation Project (22JR5RA221).

凭借着与电力系统相同的供电方式, 具有更高的应用和研究价值. 但传统交流微电网中各逆变器采用的并联接入方式会使系统内部存在着谐波和环流难以抑制, 输出电能质量较差等问题^[3-4]. 同时, 现有通过串联方式组成的微电网也不可避免地存在诸如系统内部环流难以抑制, 或微源利用率较低的缺点.

为解决或简化现有交流微电网中存在的问题, 有学者从拓扑结构出发, 提出一种半桥变流器串联星型结构微电网(half-bridge converter series Y-connection microgrids, HCSY-MG). HCSY-MG系统通过串联结构星型连接的方式将各微源半桥变流器组成三相逆变环节, 在拓扑结构层面上不仅解决了传统交流微电网中由于各变流器之间并联产生的环流问题, 而且提高了输出电压与电流中谐波的频率, 使谐波分量更容易被滤除. 同时, HCSY-MG系统采用的半桥变流器可以显著降低系统控制的难度, 提高各可再生能源的能量利用率^[5]. 但该系统由于不存在公共直流母线, 所以各可再生能源的随机性和波动性会不可避免地影响HCSY-MG系统输出电压与电流. 针对HCSY-MG系统这一种新型的微电网系统, 目前仅有研究该系统在微源输出功率严重不平衡条件下的并网功率平衡控制策略^[6], 但对其在可再生能源波动条件下并网电流的特性分析, 以及对应的控制策略却鲜有研究.

微电网在并网运行时, 由于其输出电压受电网电压控制, 故并网系统的控制目标是输出功率或电流随给定值变化^[7]. 为获得谐波含量更少、跟踪误差更低的并网电流, 在交流微电网的并网逆变器中常用重复控制、非线性无源控制、模型预测控制等方法^[8-10]. 其中, 模型预测控制(model predictive control, MPC)在应用至微电网控制及调度领域时, 具有以下优势: 有限时域内对目标函数进行优化, 滚动式地求解最优控制变量; 保持某控制时段内的最优, 而非全局最优, 以适应环境的不确定性^[11]. 基于以上优势, MPC在非线性电力变换系统中得到了广泛应用^[12], 例如与HCSY-MG系统拓扑结构类似的级联H桥变流器^[13-14]、模块化多电平变流器^[15-16]以及模块化多电平矩阵变流器^[17]等. HCSY-MG系统作为一种新型的交流微电网系统, 当可再生能源的随机性和波动性造成各相发电模块直流侧电压之和发生波动时, 其并网电流会表现出独有的特征. MPC凭借其中的预测模型和滚动优化环节, 能更有针对性地解决具有不确定性因素的优化控制问题^[18], 所以在应用至含有大量可再生能源的HCSY-MG系统并网电流控制领域中具有一定的优势.

尽管MPC在各领域都表现良好, 但其中滚动优化环节的快速性是制约其进一步发展的关键问题^[19]. 文献[20]通过提出一种改进RRT*的优化算法, 显著加快了优化环节的收敛速度, 并基于MPC设计了航迹规

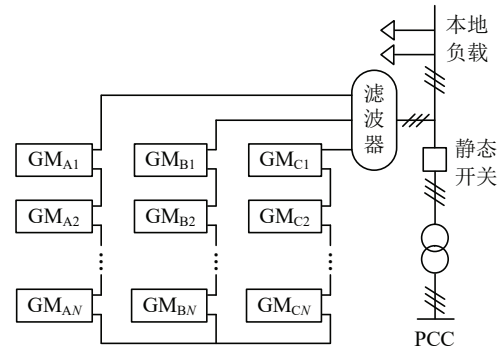
划策略, 有效降低了无人机在线航迹规划任务中的代价. 目前, 滚动优化环节常用的优化策略有启发式优化算法、凸/非凸优化算法、混合整数二次规划、整数非线性优化等^[21]. 其中, 随着启发式优化算法经过长时间发展, 收敛速度更快, 优化效果更优的算法已被提出, 可以更好地促进MPC在各场景的应用. 青蒿素优化(Artemisinin Optimization, AO)算法作为一种新型的元启发式优化算法, 随着被提出的同时, 在IEEE CEC 2014和20222基准函数测试集上与8种经典优化算法和8种高性能改进优化算法进行对比, 结果均显示AO算法有着更快的收敛速度和更好的寻优效果^[22]. 所以, 为保证滚动优化环节的快速性, AO算法可以作为MPC中滚动优化环节的优化算法.

综上所述, 本文将以HCSY-MG并网系统为研究对象, 在微源出力随机性造成并网电流存在波动的情况下, 以并网电流数学模型和特性为基础, 提出一种波动量自适应补偿的并网电流MPC策略. 在MPC的滚动优化环节采用青蒿素优化(Artemisinin Optimization, AO)算法, 并以提升算法收敛速度和降低陷入局部最优风险为目的对其进行改进. 最后, 通过仿真和实验与由重复控制和PI控制构成的复合控制策略进行对比, 验证本文所提HCSY-MG系统并网电流MPC策略的有效性、可行性和针对性.

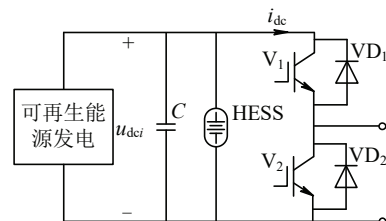
2 HCSY-MG并网系统及其特性

2.1 HCSY-MG并网系统拓扑结构

HCSY-MG系统以分布式可再生能源发电模块(generation sub-module, GM)为基本模块, 采用串联结构星型连接方式组成三相逆变环节, 并经过滤波器连接至交流母线和本地负载. HCSY-MG系统作为一种新型的微电网系统, 能够在灵活为本地负载提供电能的同时, 将多余电能输送至大电网. HCSY-MG系统结构、GM的拓扑结构如图1所示.



(a) HCSY-MG系统结构



(b) GM结构

图 1 HCSY-MG系统拓扑结构

Fig. 1 HCSY-MG system topology

由图1(b)可以看出每个GM包括可再生能源发电模块、稳压电容 C 、混合储能系统(hybrid energy storage system, HESS)和由功率开关器件 V_1, V_2 组成的半桥变流器。

可再生能源发电模块一般由光伏发电和风力发电组成,其出力会不可避免地具有随机性,造成HCSY-MG系统输出电压的波动,从而在并网电流中也存在相应的波动量。在微电网中,目前广泛采用配置储能环节的手段,解决由于可再生能源随机性和波动性造成的系统输出电压波动。尽管GM直流侧电压的波动可以由分布式HESS平抑,但仍存在着小幅度的波动,影响HCSY-MG系统并网电流的质量。所以,为进一步降低可再生能源随机性和波动性对HCSY-MG系统并网电流的影响,需要在并网电流的控制中对其波动量进行自适应补偿。

将每个GM等效为受控电压源,可得HCSY-MG并网系统的等效电路如图2所示。图中, u_{xO} 为三相逆变环节输出电压;滤波器为LCL型; R_e 为线路等效电阻; i_x 为系统输出电流; $u_{xN'}$ 为本地负载电压; i_{Lx} 为负载电流; i_{ex} 为并网电流; e_x 为电网电压。其中, $x=A, B, C$ 。

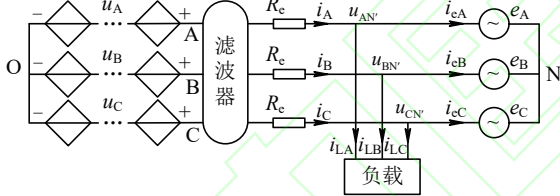


图 2 HCSY-MG并网系统的等效电路

Fig. 2 Equivalent circuit of HCSY-MG grid-connected system

2.2 并网电流数学模型及其特性分析

基于图2的并网系统等效电路,文献[23]给出了在载波移相正弦脉宽调制策略(Carrier Phase Shift - Sine Pulse Width Modulation, CPS-SPWM)下半桥变流器输出电压的表达式。在忽略高次谐波后,HCSY-MG系统单相输出电压 u_{AO} 可表示为:

$$u_{AO} = \sum_{i=1}^N u_A(i) = \frac{u_{dcA}}{2} + \frac{M \cdot u_{dcA}}{2} \sin(\omega_0 t + \varphi_A). \quad (1)$$

式中, $u_{dcx} = \sum_{i=1}^N u_{dcx}(i)$ 为逆变侧 x 相的直流侧电压之和; M 为调制比; ω_0 为调制波角频率。

由上式可以看出,当可再生能源波动造成各相直流侧电压之和不相等时,系统输出电压和并网电流中将包含直流和基频波动,进而降低跟踪给定值的精度,同时影响控制系统的稳定性。

为便于分析HCSY-MG并网电流的特性,将图2所示的并网系统等效电路转换为等效单相电路,如图3所示。

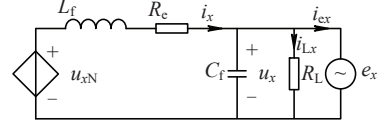


图 3 HCSY-MG并网系统等效单相电路

Fig. 3 Single-phase equivalent circuit of HCSY-MG grid-connected system

由图3可得等效单相并网系统的KVL方程为:

$$u_{xN} = L_f \frac{di_x}{dt} + R_e i_x + e_x. \quad (2)$$

令 $u_{xN} - e_x = \Delta u_x$, $i_{ex} = i_x - i_{Lx}$ 可得到三相并网电流的矩阵表达式为:

$$L_f \frac{d}{dt} \begin{bmatrix} i_{eA} \\ i_{eB} \\ i_{eC} \end{bmatrix} + \begin{bmatrix} R_e & 0 & 0 \\ 0 & R_e & 0 \\ 0 & 0 & R_e \end{bmatrix} \begin{bmatrix} i_{eA} \\ i_{eB} \\ i_{eC} \end{bmatrix} = \begin{bmatrix} \Delta u_A \\ \Delta u_B \\ \Delta u_C \end{bmatrix}. \quad (3)$$

由式(3)可以看出,影响并网电流的决定性因素为微电网输出电压与电网电压之差,即 Δu_x 。但又因为电网电压 e_x 恒定,所以影响HCSY-MG系统并网电流的关键变量之一为微电网输出电压 u_{xN} 。

设系统状态为 $u_{dcA} \neq u_{dcB} \neq u_{dcC}$, $\varphi_A=0$, $\varphi_B=-2\pi/3$, $\varphi_C=2\pi/3$ 。此时,在CPS-SPWM调制策略下,忽略高次谐波,仅考虑直流与基频分量,可以得到微电网输出电压的表达式为:

$$u_{AN} = \frac{2u_{AO} - u_{BO} - u_{CO}}{3} = \frac{1}{3} \left[\frac{2u_{dcA} - u_{dcB} - u_{dcC}}{2} + M \left(u_{dcA} + \frac{1}{4}u_{dcB} + \frac{1}{4}u_{dcC} \right) \sin \omega_0 t + \frac{\sqrt{3}}{4} M (u_{dcB} - u_{dcC}) \cos \omega_0 t \right]. \quad (4)$$

$$u_{BN} = \frac{2u_{BO} - u_{AO} - u_{CO}}{3} = \frac{1}{3} \left[\frac{2u_{dcB} - u_{dcA} - u_{dcC}}{2} + M \left(-\frac{1}{2}u_{dcA} - \frac{1}{2}u_{dcB} + \frac{1}{4}u_{dcC} \right) \sin \omega_0 t - \frac{\sqrt{3}}{4} M (2u_{dcB} + u_{dcC}) \cos \omega_0 t \right]. \quad (5)$$

$$u_{CN} = \frac{2u_{CO} - u_{AO} - u_{BO}}{3} = \frac{1}{3} \left[\frac{2u_{dcC} - u_{dcA} - u_{dcB}}{2} + M \left(-\frac{1}{2}u_{dcA} + \frac{1}{4}u_{dcB} - \frac{1}{2}u_{dcC} \right) \sin \omega_0 t + \frac{\sqrt{3}}{4} M (u_{dcB} + 2u_{dcC}) \cos \omega_0 t \right]. \quad (6)$$

由式(4)-(6)可以看出,在可再生能源波动造成三相直流侧电压不相等时,HCSY-MG系统输出电压中

会包含有直流波动量 u_z 和基频波动量 u_s . 根据式(3), 在并网电流中同样会出现直流波动量 i_z 和基频波动量 i_s . 因为并网电流常在dq坐标系下进行控制, 所以需要得到并网电流在dq坐标系下的表达式, 在有针对性地对波动量进行补偿的同时, 实现dq轴分量的解耦.

将式(4)-(6)转换至dq坐标系, 可以得到:

$$u_{zd} = \frac{1}{6} \begin{bmatrix} 2u_{dcA} - u_{dcB} - u_{dcC} \\ -\sqrt{3}u_{dcB} + \sqrt{3}u_{dcC} \end{bmatrix}^T \begin{bmatrix} \sin \omega_0 t \\ \cos \omega_0 t \end{bmatrix}. \quad (7)$$

$$u_{zq} = \frac{1}{6} \begin{bmatrix} \sqrt{3}u_{dcB} - \sqrt{3}u_{dcC} \\ 2u_{dcA} - u_{dcB} - u_{dcC} \end{bmatrix}^T \begin{bmatrix} \sin \omega_0 t \\ \cos \omega_0 t \end{bmatrix}. \quad (8)$$

$$u_{sd} = \frac{2M}{3} \begin{bmatrix} \frac{1}{12}u_{dcA} + \frac{5}{24}u_{dcB} + \frac{5}{24}u_{dcC} \\ \frac{\sqrt{3}}{8}u_{dcB} - \frac{\sqrt{3}}{8}u_{dcC} \\ -\frac{1}{4}u_{dcA} + \frac{1}{8}u_{dcB} + \frac{1}{8}u_{dcC} \end{bmatrix}^T \begin{bmatrix} 1 \\ \sin 2\omega_0 t \\ \cos 2\omega_0 t \end{bmatrix}. \quad (9)$$

$$u_{sq} = \frac{2M}{3} \begin{bmatrix} \frac{1}{4}u_{dcA} - \frac{1}{8}u_{dcB} - \frac{1}{8}u_{dcC} \\ \frac{\sqrt{3}}{8}u_{dcB} - \frac{\sqrt{3}}{8}u_{dcC} \end{bmatrix}^T \begin{bmatrix} \sin 2\omega_0 t \\ \cos 2\omega_0 t \end{bmatrix}. \quad (10)$$

式中, u_{zd} 、 u_{zq} 、 u_{sd} 和 u_{sq} 分别为系统输出电压中包含的直流和基频波动量在dq坐标系下的表达形式.

由式(7)-(10)可以看出, 在可再生能源波动造成三相直流侧电压不相等时, HCSY-MG系统输出电压中的直流和基频波动量在dq坐标系下会表现为50Hz和100Hz的波动量. 同理, 并网电流中也存在相同频率的波动量, 可以表示为:

$$i_{zd} = i_1 \sin \omega_0 t + i_2 \cos \omega_0 t. \quad (11)$$

$$i_{zq} = i_3 \sin \omega_0 t + i_4 \cos \omega_0 t. \quad (12)$$

$$i_{sd} = i_5 + i_6 \sin 2\omega_0 t + i_7 \cos 2\omega_0 t. \quad (13)$$

$$i_{sq} = i_8 \sin 2\omega_0 t + i_9 \cos 2\omega_0 t. \quad (14)$$

式中, i_{zd} 、 i_{zq} 、 i_{sd} 和 i_{sq} 分别为并网电流中包含的直流和基频波动量在dq坐标系下的表达形式; $i_1 \sim i_9$ 为相应频率波动量的系数.

由以上HCSY-MG系统并网电流的数学模型可以分析总结出其特性为:

(1)影响HCSY-MG系统并网电流的关键变量为各相GM直流侧电压之和.

(2)当可再生能源出力存在波动时, 会使得各相GM直流侧电压之和同样出现波动, 进而会造成并网电流中包含有直流分量和基频偏差量.

(3)系统输出电压和并网电流中包含的直流分量和基频偏差量在dq坐标系下表现为50Hz和100Hz的波动量.

3 波动量自适应补偿的并网电流模型预测控制

由图1所示的HCSY-MG系统拓扑结构可以看出, 因为该系统的各相GM直流侧不存在公共直流链, 所以可再生能源出力波动对直流侧电压之和的影响会更为严重. 在对HCSY-MG系统并网电流进行控制时, 必须要考虑到上述特性. MPC由于包含着滚动优化和预测模型, 适用于存在大量可再生能源的HCSY-MG系统, 故本节将研究一种波动量自适应补偿的并网电流MPC策略. 同时, 为提高滚动优化环节的收敛速度和降低算法陷入局部最优的概率, 对滚动优化环节使用的AO算法进行改进.

3.1 HCSY-MG系统并网电流预测模型

MPC策略中广泛采用的预测模型包括有微分方程、差分方程、状态方程和传递函数等^[23], 本节结合2.2节建立的并网电流数学模型, 给出HCSY-MG系统并网电流MPC策略中采用的预测模型. 根据得到的dq坐标系下的控制变量 E_d 、 E_q , 经过2/3变换后得到abc坐标系下的三相调制波 E_A 、 E_B 、 E_C , 再通过式(1)、(4)-(6), 可得到HCSY-MG系统输出电压, 最后经式(3)得到三相并网电流预测值. 并网电流预测模型的示意图如图4所示.



图4 HCSY-MG系统并网电流预测模型示意图

Fig. 4 Schematic diagram of grid-connected current prediction model for HCSY-MG system

3.2 反馈校正及优化问题

在含有大量可再生能源的HCSY-MG系统中, 由于可再生能源的随机性和波动性, 并网电流预测模型无法准确刻画未来结果. 所以, 需要加入反馈校正环节以降低可再生能源波动性对MPC的影响, 即通过修正预测模型的输出, 提高预测模型的精度. 本文所使用的反馈校正可以表示为:

$$i'_d = 0.5i_d + 0.5\hat{i}_d. \quad (15)$$

$$i'_q = 0.5i_q + 0.5\hat{i}_q. \quad (16)$$

式中, i'_d 、 i'_q 分别为并网电流经反馈校正后的值; i_d 、 i_q 分别为并网电流经3/2变换后的实际值; \hat{i}_d 、 \hat{i}_q 分别为预测模型输出并网电流经3/2变换后的预测值.

为达到准确跟踪并网电流给定值的目的, 取二次型最优化函数作为滚动优化环节的目标函数, 即:

$$\min J(k) = [\Delta i_d(k+i|k)]^T P [\Delta i_d(k+i|k)] + [\Delta i_q(k+i|k)]^T Q [\Delta i_q(k+i|k)]. \quad (17)$$

式中, k 为当前时刻; i 为预测步长; $P = \text{diag}[0.5, 0.5, \dots, 0.5]$, $Q = \text{diag}[0.5, 0.5, \dots, 0.5]$ 为加权对角矩阵; Δi_d 和 Δi_q 的表达式为:

$$\begin{cases} \Delta i_d = i_{d\text{ref}} - i'_d \\ \Delta i_q = i_{q\text{ref}} - i'_q \end{cases} \quad (18)$$

式中, $i_{d\text{ref}}$ 、 $i_{q\text{ref}}$ 分别为并网电流 dq 轴分量的目标值。

同时, 为保证并网电流控制的精度, 减轻可再生能源出力波动对HCSY-MG系统并网电流的影响, 需要补偿如式(11)-(14)所示的50Hz和100Hz的波动量。并且, 为提升 q 轴电流对于给定值的静态跟踪效果, 将式(14)重写为:

$$i'_{sq} = i_8 + i_9 \sin 2\omega_0 t + i_{10} \cos 2\omega_0 t. \quad (19)$$

进而可得到带有补偿量的控制变量为:

$$\begin{cases} E_d = i_{zd} + i_{sd} \\ E_q = i_{zq} + i'_{sq} \end{cases} \quad (20)$$

从式(20)可以看出, 滚动优化环节需要输出的最优补偿系数共10个, 分别对应为式(11)-(13)、(19)中各频率波动量的系数。为避免混淆, 设滚动优化环节输出的最优补偿系数为 $x_1 \sim x_{10}$ 。此外, 根据式(20)给出的控制变量可以看出, 此时并网电流在 dq 坐标系下的分量实现了完全解耦, 即二者之间不存在任何耦合关系, 可以显著提高控制系统的效果。

由3/2变换和2/3变换的理论可知, 三相正弦量在经过3/2变换后, d 轴分量等于三相正弦量的幅值。为保证HCSY-MG系统运行的安全, 并网电流不能超过各元件的最大承受限度。所以, 将输出约束转换为状态约束, 即设置MPC策略中滚动优化环节输出补偿量 $x_1 \sim x_{10}$ 的范围为 $[-80, 80]$ 。

3.3 基于改进AO算法的滚动优化

滚动优化环节作为MPC策略中的一个重要组成部分, 其快速性和寻优效果成为制约MPC发展的瓶颈。因为AO算法更快的收敛速度和更优的寻优结果, 所以本文将采用AO算法作为MPC中滚动优化环节的核心算法。

AO算法中共包括了4个阶段, 分别为初始化阶段、综合淘汰阶段、局部清除阶段和后巩固阶段。其中, 初始化阶段的搜索代理可以表示为:

$$A_{N,D} = B + R(T - B) = \begin{bmatrix} a_{11} & \cdots & a_{1D} \\ \vdots & \ddots & \vdots \\ a_{N1} & \cdots & a_{ND} \end{bmatrix}. \quad (21)$$

式中, A 为初始化的种群; N 为种群数量; D 为搜索代理

的维度; T 和 B 分别为搜索空间的上下界; $R \in [0, 1]$ 为随机数序列。

综合淘汰阶段的搜索代理更新过程为:

$$a_{i,j}^{t+1} = \begin{cases} a_{i,j}^t + (-1)^t c \cdot a_{i,j}^t, \text{rand} < 0.5 \\ a_{i,j}^t + (-1)^t c \cdot \text{best}_j^t, \text{rand} > 0.5 \end{cases}, r_1 < K. \quad (22)$$

式中, $a_{i,j}^t$ 和 $a_{i,j}^{t+1}$ 分别为更新前后的搜索代理; best_j^t 为当前最优; c 为药物在人体内的浓度衰减系数; $r_1 \in [0, 1]$ 为一随机数; K 为一概率系数, 表示该阶段持续时间的差异。

局部清除阶段的搜索代理更新过程可以表示为:

$$a_i^{t+1} = a_{b3}^t + d(a_{b1}^t - a_{b2}^t), \text{rand} < f_{\text{norm}}(i). \quad (23)$$

式中, $f_{\text{norm}}(i)$ 为归一化的适应度值; $d \in [0.1, 0.6]$ 为一随机值; $b1, b2, b3$ 满足如下条件:

$$b1, b2, b3 \sim U(1, N), b1 \neq b2 \neq b3. \quad (24)$$

后巩固阶段的搜索代理更新过程可以表示为:

$$a_{i,j}^{t+1} = \begin{cases} a_{i,j}^t, \text{rand} < 0.05 \\ \text{best}_{i,j}, \text{rand} < 0.2 \end{cases} \quad (25)$$

通过对AO算法基本原理的叙述可以发现, 在初始化阶段中, 搜索代理是通过随机参数 R 实现初始化。文献[24]指出该随机初始策略会导致种群多样性较弱, 且搜索代理在迭代过程中易陷入局部最优, 所以利用Tent映射对麻雀搜索优化算法的种群进行混沌化, 并提出一种有效的混沌麻雀搜索优化算法。关于Tent混沌映射的有效性, 文献[25]通过严格的数学推理, 证明了Tent映射能够有效混沌化优化算法中的种群, 并且相比于Logistic映射, 有着更优的遍历性和收敛速度。所以, 本文将采用Tent映射混沌化AO算法的初始种群, 以提升初始化种群的多样性和随机性, 降低搜索代理陷入局部最优的风险。Tent映射的数学表达式为:

$$a^{k+1} = \begin{cases} \frac{a^k}{\beta}, a^k \in (0, \beta] \\ \frac{1 - a^k}{1 - \beta}, a^k \in (\beta, 1] \end{cases} \quad (26)$$

式中, β 为混沌因子。

混沌化前后的初始化种群示意图如图5所示。

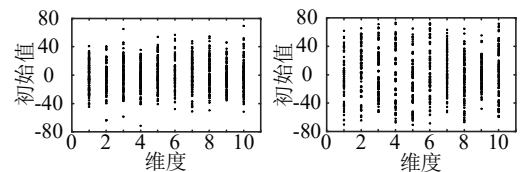


图5 混沌化前后的初始化种群

Fig. 5 Initialized populations before and after chaoticization

由图5可以看出, 混沌化前的初始化种群分布大

多集中随机分布在 $[-40,40]$ 区间内,在 $[-80,-40]$ 和 $[40,80]$ 区间内存在的搜索代理数量较少;但混沌化后的初始化种群能够更均匀地分布在 $[-80,80]$ 区间内。以上结果证明了所采用的Tent混沌映射可以有效提升初始化种群在待搜索空间内的随机性和遍历性。

同时,统计分析了AO算法除初始化阶段之外的3个核心阶段,各阶段在优化迭代过程中的平均占比分别为:综合淘汰阶段占15%,局部清除阶段占57%,后巩固阶段占28%。由此可见,局部清除阶段占据了大多数迭代过程,说明在该阶段可能会陷入局部最优,并且收敛缓慢。所以,本小节将使用自适应更新策略改进式(23)中参数 d 的选择。

在改进策略中,通过比较搜索代理在当前迭代中适应度值与前一次迭代中平均适应度值的大小,以确定参数 d 的自适应更新方式。该策略可以表示为:

$$d = \begin{cases} d_{\max}, & \text{other} \\ d_{\min} + \frac{(f(i) - f_{\min})(d_{\max} - d_{\min})}{f_{\text{ave}} - f_{\min}}, & f(i) < f_{\text{ave}}. \end{cases} \quad (27)$$

式中, d_{\min} 与 d_{\max} 分别为参数 d 的最小值与最大值,即0.1与0.6; $f(i)$ 为当前适应度值; f_{\min} 为适应度值的最小值; f_{ave} 为适应度值的平均值。

若搜索代理的更新方式按式(23)进行,搜索代理的更新步长为 d ,但 d 为一随机数,所以更新步长不受控制,导致搜索代理不能更快收敛至最优解。若搜索代理更新方式中的参数 d 按式(27)所示的自适应更新方式时,参数 d 的更新步长将受到 $f(i)$,即当前适应度值的影响。当 $f(i) < f_{\text{ave}}$ 时,说明此时的搜索代理能达到较小的适应度值,即有着更优的寻优结果,此时应加速收敛,并且在加速收敛的同时突破可能存在的局部最优。当 $f(i) > f_{\text{ave}}$ 时,说明此时的搜索代理不能收敛到一个较优的结果,此时不能取过小的 d ,以保证搜索代理的探索性,防止无法收敛至最优值。

随后,结合3.2小节给出的滚动优化环节输出的最优补偿系数 $x_1 \sim x_{10}$,设改进AO算法中的搜索代理维度 $\text{dim}=10$ 。最后,根据3.1小节所给出的并网电流预测模型、3.2小节给出的反馈校正及优化问题、3.3小节提出的基于改进AO的滚动优化环节,可以得到如图6所示的HCSY-MG系统并网电流MPC策略框图。

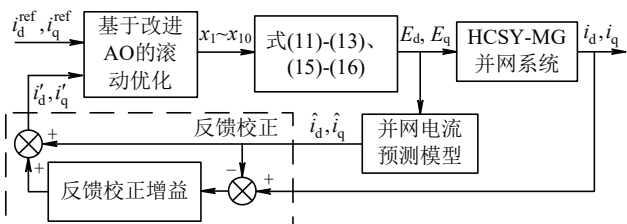


图6 HCSY-MG系统并网电流MPC策略框图

Fig. 6 Block diagram of grid-connected current MPC strategy

for HCSY-MG system

由图6所示的HCSY-MG系统并网电流MPC策略可以看出,所提出的策略是根据HCSY-MG并网电流特性提出的,即如式(20)所示的最优控制序列。同时,可以实现dq轴分量的完全解耦,提高并网电流的控制效果与精度。下文将通过仿真和实验对比,证明本节所提出MPC策略的有效性、可行性和优越性。

4 仿真实验

为验证本文所提基于波动量自适应补偿的HCSY-MG系统并网电流模型预测控制在可再生能源波动条件下的可行性和有效性,搭建了相应的仿真模型,并与重复控制和PI控制构成的复合控制进行对比验证。仿真中的主要参数如表1所示。

表1 仿真中的主要参数

Table 1 The main parameters in the simulation

| 参数 | | 数值 |
|-------------|-----------|------------|
| HCSY-MG系统参数 | 变流器侧滤波电感 | 1mH |
| | 网侧滤波电感 | 0.1mH |
| | 滤波电容 | 20μF |
| | 线路等效电阻 | 1Ω |
| | 载波频率 | 10kHz |
| AO算法主要参数 | 种群数量 | 30 |
| | 迭代次数 | 50 |
| | 上下限约束 | $[-80,80]$ |
| | 混沌因子 | 0.7 |
| 复合控制主要参数 | 搜索代理维度 | 10 |
| | 重复控制增益 | 3.5 |
| | 超前环节步数 | 6 |
| | 二阶滤波器截止频率 | 1kHz |
| | 比例环节增益 | 10 |
| | 积分环节增益 | 500 |

4.1 直流侧电压之和不相等

由于HCSY-MG系统各GM通过串联方式连接,所以其输出电流是相等的,当可再生能源波动造成其出力波动时,会造成其输出电压出现波动,进而造成各相GM直流侧电压之和出现波动。设置 $u_{\text{dcA}}=600\text{V}$, $u_{\text{dcB}}=u_{\text{dcC}}=640\text{V}$,用以模拟由于可再生能源随机波动造成的各相直流侧电压之和不相等的工况,同时观察本文所提MPC策略的静态特性。并网电流给定值 $i_{\text{dref}}=20\text{A}$, $i_{\text{qref}}=0\text{A}$,电网电压 $e=380\text{V}$ 。

在该种工况时,采用复合控制策略的HCSY-MG系统三相并网电流波形和 i_d 、 i_q 的波形如图7所示。由图7(a)可以看出,当可再生能源波动造成各相直流侧电压之和不相等时,采取复合控制可以使HCSY-MG系统并网电流的幅值较好地跟踪给定值,但三相并网电流的正弦度存在差异。此时 i_A 的基波分量为19.7A,跟随给定值的效果较好。但总谐波畸变率(total harmonic distortion, THD)达到了6.63%,

大于IEEE所要求的5%。此时其余两相并网电流的THD分别为6.45%, 6.42%; 三相并网电流中所包含的直流分量分别为1.33A, 0.93A, 0.41A。由该结果可以看出, 此时三相并网电流的THD均较高, 且含有一定的直流分量。观察图7(b)中的 i_d 和 i_q 曲线, 其中 i_d 曲线可以较为快速地跟随给定并保持; 但 i_q 曲线需要较长的时间才可达到给定值, 同时存在着波动。该现象说明, 在复合控制策略下, HCSY-MG系统并网电流的幅值可以较好地跟随给定值, 但其与电网电压的相位差存在着波动。

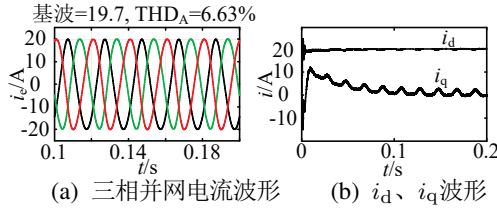


图7 工况1条件下采用复合控制策略的并网电流特征

Fig. 7 Characteristics of the grid-connected current under operating condition 1 using the composite control strategy

在同样的工况下, 采用本文所提出的HCSY-MG系统并网电流MPC策略时, 三相并网电流波形和 i_d 、 i_q 波形如图8所示。

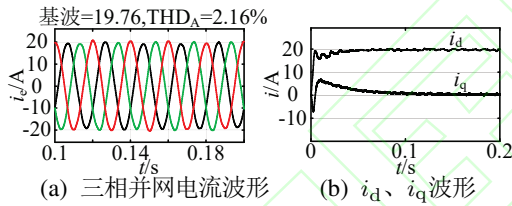


图8 工况1条件下采用MPC策略的并网电流特征

Fig. 8 Characteristics of the grid-connected current under operating condition 1 using the MPC strategy

由图8(a)可以看出, 在可再生能源波动造成各相直流侧电压之和不相等的情况下, 采用本文所提MPC策略时的并网电流幅值可以较好地跟踪给定值, 但三相并网电流的正弦度明显优于复合控制下的情况。此时 i_A 的基波分量为19.76A, 跟随给定值的效果较好, 同时THD仅为2.16%, 满足IEEE所要求的并网电流THD应小于5%。此时其余两相并网电流的THD分别为2.19%, 1.93%; 三相并网电流中所包含的直流分量分别为0.04A, 0.09A, 0.04A。由该结果可以看出, 本文所提出的MPC策略可以保证三相并网电流的THD均小于IEEE要求的5%, 同时所包含的直流分量则均有明显下降。该仿真结果说明, 当由可再生能源波动造成各相直流侧电压之和不相等时, 本文所提出的并网电流控制策略在保证并网电流质量和降低直流分量方面是有效且可行的。图8(b)的曲线可以反映出 i_d 和 i_q 曲线都可以较为快速地跟随给定值并保持。但 i_q 曲线需要较长的时间才可得到给定值并保持。相比于图7(b)中的 i_d 和 i_q 曲线, 采用本文提

出HCSY-MG系统并网电流MPC策略时的 i_q 曲线不存在周期性波动, 保证了并网电流与电网电压之间的相位差不会存在波动。

在此过程中, AO算法的适应度函数收敛曲线和搜索代理更新过程如图9所示。

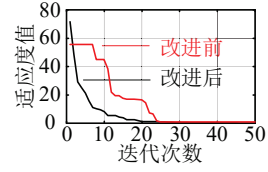


图9 AO算法迭代过程

Fig. 9 Iterative process of AO algorithm

由图9给出的AO算法改进前后的适应度值收敛过程可以看出, 改进前的适应度值收敛缓慢, 且存在斜率为零的部分, 即陷入局部最优; 改进后的适应度值收敛迅速, 可以更快地收敛至最小值。改进后的各阶段占总迭代次数的比例分别为: 综合淘汰阶段占24%, 局部清除阶段占34%, 后巩固阶段占42%。以上结果证明了本文对AO算法进行的改进是可行且有效的, 即Tent混沌映射和参数自适应更新策略能够进一步加速该算法的收敛, 并且降低陷入局部最优的风险。同时, 改进AO算法在迭代50次后, 适应度值可以收敛至0.24, 并且在20次迭代时已经收敛至接近最小值, 也证明了改进策略的有效性。最终在该工况下, 改进AO算法得到的 $x_1 \sim x_{10}$ 最优值分别为: 13.29, -0.04, -0.02, 13.33, 5.93, -0.18, -5.95, -0.2, 5.98, -0.01。

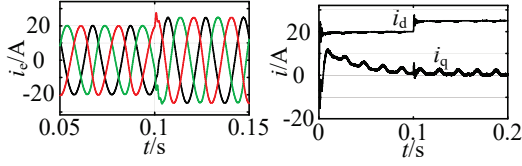
结合以上仿真结果与分析可以得到, 本文利用Tent混沌映射和参数自适应更新策略能够有效加速AO算法的收敛, 并且能够降低算法陷入局部最优的风险; 在可再生能源波动造成各相直流侧电压之和不相等时, 相较于重复控制和PI控制组成的复合控制策略, 本文所提出的波动量自适应补偿MPC策略能够使并网电流在准确跟踪给定值的基础上, 更好地保持并网电流的高质量, 同时具有更优的静态特性。

4.2 并网电流给定值变化

依旧设置系统状态为 $u_{dcA}=600V$, $u_{dcB}=u_{dcC}=640V$, 电网线电压 $e=380V$ 。并网电流给定值在0.1s之前为 $i_{dref}=20A$, $i_{qref}=0A$, 0.1s时变为 $i_{dref}=25A$ 。用以模拟在可再生能源波动造成各相直流侧电压之和不相等时, 并网电流给定值变化的工况, 同时观察本文所提MPC策略的动态特性。

此时采用复合控制策略的HCSY-MG系统三相并网电流波形和 i_d 、 i_q 的波形如图10所示。由图10(a)的三相并网电流波形可以看出, 在并网电流给定值变化的瞬间, 并网电流会出现较为剧烈的抖动, 但在短暂调整后, 其幅值可以跟随给定值。由图10(b)可以看出, i_d 和 i_q 在给定值变化时会出现较为剧烈的抖动, 但 i_d 会在短暂调整后准确跟随给定值, i_q 依旧存在着

周期性波动.同时可以发现,当 i_d 的给定值变化时, i_q 也会出现抖动,即dq轴分量存在着耦合.

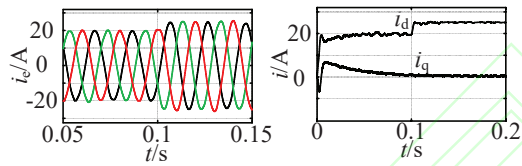


(a) 三相并网电流波形 (b) i_d 、 i_q 波形

图 10 工况2条件下采用复合控制策略的并网电流特征

Fig. 10 Characteristics of the grid-connected current under operating condition 2 using the composite control strategy

在同样的工况下,采用本文所提出的HCSY-MG系统并网电流MPC策略时,三相并网电流波形和 i_d 、 i_q 的波形如图11所示.对比图11与图10,当并网电流给定值在0.1s变化时,采用本文所提控制策略的并网电流不存在剧烈抖动,其幅值也可以很快地跟随给定值的变化,同时 i_{dref} 的变化仅会使 i_d 跟随变化,不会对 i_q 造成任何影响,证明了本文所提控制策略可以实现dq轴分量的完全解耦,并且 i_q 不存在周期性波动.



(a) 三相并网电流波形 (b) i_d 、 i_q 波形

图 11 工况2条件下采用MPC策略的并网电流特征

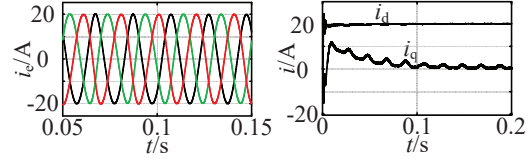
Fig. 11 Characteristics of the grid-connected current under operating condition 2 using the MPC strategy

结合以上仿真结果与分析可以得到,并网电流给定值变化时,采用本文所提MPC策略的HCSY-MG系统并网电流能够迅速跟随给定值,并且实现了dq轴分量的完全解耦,同时有着更优的动态特性.

4.3 直流侧电压之和变化

设置系统状态为 $u_{dcA}=600V$, $u_{dcB}=u_{dcC}=640V$,电网线电压 $e=380V$,并网电流给定值为 $i_{dref}=20A$, $i_{qref}=0A$. 0.1s时 u_{dcA} 由600V变为620V, u_{dcB} 由640V变为620V,用以模拟可再生能源波动造成HCSY-MG系统各相直流侧电压之和波动的工况,同时观察本文所提MPC策略的动态特性.

此时采用复合控制策略的HCSY-MG系统三相并网电流波形和 i_d 、 i_q 的波形如图12所示.由图12(a)的HCSY-MG系统三相并网电流波形可以看出,在采用复合控制时,系统直流侧电压之和的波动基本不会对并网电流的特征产生较大影响.由图12(b)的 i_d 和 i_q 曲线可以看出,系统直流侧电压之和的波动对 i_d 基本没有影响,但可明显发现会使 i_q 的波动量减小,即仍会造成并网电流与电网电压之间存在相位波动.

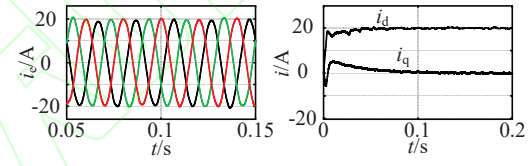


(a) 三相并网电流波形 (b) i_d 、 i_q 波形

图 12 工况3条件下采用复合控制策略的并网电流特征

Fig. 12 Characteristics of the grid-connected current under operating condition 3 using the composite control strategy

在同样的工况下,当采取本文所提出的HCSY-MG系统并网电流MPC策略时,三相并网电流波形和 i_d 、 i_q 的波形如图13所示.由图13(a)可以看出,各相直流侧电压之和在0.1s变化时,采用本文所提控制策略的并网电流基本不存在变化.同时,从图13(b)可以看出, i_d 和 i_q 依然可以较为准确地跟踪给定值,并且在直流侧电压之和变化的时刻没有出现较大波动,对比图13与图12,本文所提出的并网电流MPC策略在各相直流侧电压之和波动时,可以使HCSY-MG系统的并网电流保持良好的动态特性.



(a) 三相并网电流波形 (b) i_d 、 i_q 波形

图 13 工况3条件下采用MPC策略的并网电流特征

Fig. 13 Characteristics of the grid-connected current under operating condition 3 under the MPC strategy

以上三种工况下的仿真结果证明,在可再生能源存在波动性的情况下,相比于重复控制和PI控制构成的复合控制策略,本文所提出的并网电流MPC策略均能够使并网电流较为准确且稳定地跟踪给定值.同时,该策略不仅可以实现dq轴分量的完全解耦,而且能够提高控制效果,而且其静态和动态过程更优.此外,所采用的Tent混沌映射和参数自适应更新策略不仅可以加速AO算法的收敛,而且可以降低算法选入局部最优的概率.以上结果均证明了本文所提方法具有可行性和有效性.

5 实验验证

为验证HCSY-MG拓扑结构以及本文所提并网电流控制策略的可行性和有效性,搭建了相应的实验平台. HCSY-MG并网实验平台的主要参数为:每相GM个数 $N=4$, GM直流侧电压 $u_{dc}=80V$,并网点线电压 $e=110V$,载波频率 $f_c=10kHz$,补偿量范围 $[-5,5]$.实验平台如图14所示.

设置A相直流侧电压之和 $u_{dcA}=310V$,其余两相 $u_{dcB}=u_{dcC}=320V$,用以模拟可再生能源波动造成各相直流侧电压之和不相等的工况.

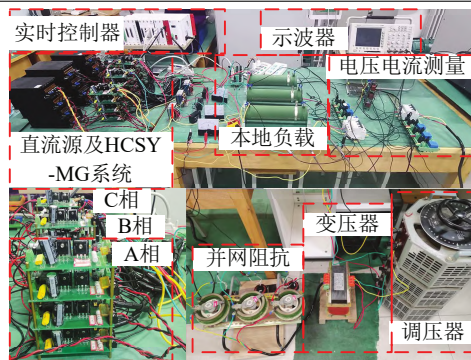


图 14 实验平台照片

Fig. 14 Photo of experimental platform

此时采用复合控制策略的HCSY-MG系统三相并网电流实验波形, 以及A相并网电流与电网电压波形如图15所示。

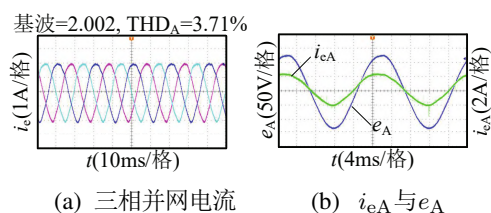


图 15 复合控制策略下的并网电流实验特征

Fig. 15 Experimental characteristics of the grid-connected current under the composite control strategy

由图15(a)的HCSY-MG系统并网电流实验波形可以看出, 并网电流的幅值可以较为准确地跟踪给定值且保持稳定. 此时的基频分量为2.002A, THD=3.71%, 其中对电流给定值的跟踪误差为0.002A. 尽管基波分量可以较好地达到给定值, 但其THD较大, 所以复合控制策略在对HCSY-MG系统并网电流进行控制时存在着一定缺陷. 观察图15(b)中电网电压与并网电流波形可以看出, 尽管并网电流的相位可以较为准确地与电网电压保持同步, 但二者上升段的过零点存在一定的偏差。

由于实时控制器的运算能力有限, 首先在离线条件下得到相应的最优补偿系数 $x_1 \sim x_{10}$ 分别为: 3.31, 0.03, 0.01, 3.32, 1.42, -0.03, -1.48, 0.19, 1.49, 0.01. 随后将上述最优参数带入本文所提并网电流控制策略中, 此时的HCSY-MG系统三相并网电流波形, 以及A相并网电流与电网电压波形如图16所示。

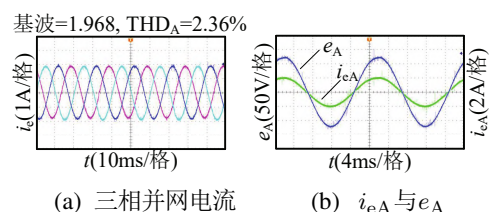


图 16 MPC策略下的并网电流实验特性

Fig. 16 Experimental characteristics of the grid-connected current under the MPC strategy

由图16(a)的三相并网电流波形可以看出, 其幅值均可以较为准确地跟踪给定值, 且正弦度良好. 此时的基波分量为1.968A, THD=2.36%. 相较于复合控制, 尽管电流幅值的跟踪精度略有下降, 但THD明显更优. 观察图16(b)的A相电网电压与并网电流波形可以发现, 并网电流的相位可以准确地与电网电压保持同步. 与图15(b)对比可以看出, 二者上升段的过零点不存在偏差, 故本文提出的并网电流控制策略可以更好地保证并网电流与电网电压的相位一致。

以上实验结果证明, 与重复控制和PI控制构成的复合控制策略相比, 本文所提出的并网电流MPC策略不仅可以使得并网电流更为准确地跟踪给定值, 而且可以实现dq轴分量的完全解耦控制, 同时静态和动态特性更优. 综上, 本文所提出的HCSY-MG系统并网电流波动量自适应补偿MPC策略是可行的、有效的, 同时更具有针对性。

6 结论

本文为降低各相直流链电压之和不相等对并网电流稳定性的影响, 以及提高HCSY-MG系统并网电流控制的精度, 有针对性地提出一种并网电流波动量自适应补偿的模型预测控制策略. 同时, 为提升模型预测控制中滚动优化环节的收敛速度和寻优效率, 提出一种改进AO算法, 并通过仿真验证了改进策略的有效性和可行性. 最后, 通过仿真和实验对比分析了本文所提MPC策略与重复控制和PI控制构成的复合控制策略, 证明了本文应用模型预测控制解决HCSY-MG系统并网电流控制问题具有以下优势: 在可再生能源出力波动造成各相直流侧电压之和不相等、直流侧电压之和波动、并网电流给定值变化的情况下, 能有效提高并网电流对于给定值的跟踪精度; 在实现dq轴控制分量完全解耦的同时, 保证更优的静态和动态特性; 更能适应可再生能源的波动和HCSY-MG系统的特殊性。

然而, 本文并未考虑HCSY-MG系统各相直流侧电压之和不相等的极限. 因此, 在保证系统安全稳定运行的前提下, 还需要研究各相直流侧电压之和不相等的极限, 以及越限以后的并网电流控制策略。

参考文献:

- [1] PANWAR N L, KAUSHIK S C, KOTHARI S. S Role of Renewable Energy Sources in Environmental Protection: A Review. *Renewable & Sustainable Energy Reviews*, 2011, 15(3): 1513 – 1524.
- [2] CARTON J G, OLABI A G. Wind/Hydrogen Hybrid Systems: Opportunity for Ireland's Wind Resource to Provide Consistent Sustainable Energy Supply. *Energy*, 2010, 35(12): 4536 – 4544.
- [3] FENG Wei, SUN Kai, GUAN Yajuan, et al. A harmonic current suppression strategy for voltage source grid-connected inverters based on output voltage hybrid control in islanded microgrids. *Transactions of China Electrotechnical Society*, 2016, 31(7): 72 – 80.

(冯伟, 孙凯, 关雅娟, 等. 孤立微电网中基于输出电压复合控制的电

- 压源型并网逆变器谐波电流抑制策略. 电工技术学报, 2016, 31(7): 72 – 80.)
- [4] TU Chunming, YANG Yi, XIAO Fan, et al. The output side power quality control strategy for microgrid main inverter under nonlinear load. *Transactions of China Electrotechnical Society*, 2018, 33(11): 2486 – 2495.
(涂春鸣, 杨义, 肖凡, 等. 非线性负载下微电网主逆变器输出侧电能质量控制策略. 电工技术学报, 2018, 33(11): 2486 – 2495.)
- [5] WANG X G, LI J J, GUO Q, et al. Parameter Design of Half-Bridge Converter Series Y-Connection Microgrid Grid-Connected Filter Based on Improved PSO-LSSVM. *International Transactions on Electrical Energy Systems*, 2023: 1 – 13.
- [6] WANG Xinggui, LI Yu, LI Jinjian, et al. Power Balance Control Strategy for HCSY-MG Based on Trapezoidal Wave Compensation and Power Adaptation. *Proceeding of the CSEE*, 2024, 2: 1 – 13.
(王兴贵, 李昱, 李锦键, 等. 基于梯形波补偿和功率自适应的HCSY-MG功率平衡控制策略. 中国电机工程学报, 2024, 2: 1 – 13.)
- [7] GUAN M Y, XU Z. Modeling and Control of a Modular Multilevel Converter-Based HVDC System Under Unbalanced Grid Conditions. *IEEE Transactions on Power Electronics*, 2012, 27(12): 4858 – 4867.
- [8] LAN Ziran, HAO Ruixiang, JIAO Honglin, et al. Optimal Preview Control of Three-phase Inverter Based on Repetitive Control and State-Feedback. *Transactions of China Electrotechnical Society*, 2022, 37(6): 1473 – 1481.
(兰梓冉, 郝瑞祥, 角宏林, 等. 基于重复控制和状态反馈的三相逆变器最优预见控制. 电工技术学报, 2022, 37(6): 1473 – 1481.)
- [9] WANG Xinggui, WANG Hailiang, XUE Sheng, et al. Grid-connected current control for MMC-MG adopting nonlinear passive theory. *Control Theory & Applications*, 2022, 39(8): 1541 – 1550.
(王兴贵, 王海亮, 薛晟, 等. 采用非线性无源理论的MMC-MG并网电流控制. 控制理论与应用, 2022, 39(8): 1541 – 1550.)
- [10] GUO Leilei, JIN Nan, LI Yanyan, et al. Grid voltage sensorless model predictive control for grid-connected inverters. *Transactions of China Electrotechnical Society*, 2020, 35(12): 2612 – 2622.
(郭磊磊, 金楠, 李琰琰, 等. 并网逆变器无电网电压传感器模型预测控制. 电工技术学报, 2020, 35(12): 2612 – 2622.)
- [11] LU Peng, YE Lin, PEI Ming, et al. Coordinated Control Strategy for Active Power of Wind Power Cluster Based on Model Predictive Control. *Proceedings of the CSEE*, 2021, 41(17): 5887 – 5899.
(路朋, 叶林, 裴铭, 等. 风电集群有功功率模型预测协调控制策略. 中国电机工程学报, 2021, 41(17): 5887 – 5899.)
- [12] WANG Lianqiang, ZHANG Li, XIONG Yongsheng, et al. Research on Three-phase Modeling MPC strategy Suitable for MMC Multi-objective Control. *Proceedings of the CSEE*, 2022, 42(S1): 287 – 294.
(王连强, 张莉, 熊永圣, 等. 适用于MMC多目标控制的三相建模MPC策略研究. 中国电机工程学报, 2022, 42(S1): 287 – 294.)
- [13] HUANG Haihong, YAN Bichen, WANG Haixin. Model Predictive Control of Current Tracking Optimization and Circulating Current Suppression for Multi-Parallel Cascaded H-Bridge Power Supplies. *Transactions of China Electrotechnical Society*, 2023, 38(16): 4376 – 4390.
(黄海宏, 颜碧琛, 王海欣. 并联级联H桥电源电流跟踪优化与环流抑制的模型预测控制. 电工技术学报, 2023, 38(16): 4376 – 4390.)
- [14] CORTÉS P, WILSON A, KOURO S, et al. Model Predictive Control of Multilevel Cascaded H-Bridge Inverters. *IEEE Transactions on Industrial Electronics*, 2010, 57(8): 2691 – 2699.
- [15] TUO P, GONG Z, ZHENG X, et al. Three-stage model predictive control for modular multilevel converters with comprehensive performance optimization. *Journal of Power Electronics*, 2024, 4: 1 – 12.
- [16] GAO X N, TIAN W, YANG Q F, et al. Model Predictive Control of a Modular Multilevel Converter Considering Control Input Constraints. *IEEE Transactions on Power Electronics*, 2024, 39(1): 636 – 648.
- [17] CUZMAR R H, MORA A, PEREDA J, et al. Long-Horizon Sequential FCS-MPC Approaches for Modular Multilevel Matrix Converters. *IEEE Transactions on Industrial Electronics*, 2024, 71(5): 5137 – 5147.
- [18] WU Chenghui, LIN Shenghong, XIA Chengjun, et al. Distributed Optimal Dispatch of Microgrid Cluster Based on Model Predictive Control. *Power System Technology*, 2020, 44(2): 530 – 538.
(吴成辉, 林声宏, 夏成军, 等. 基于模型预测控制的微电网群分布式优化调度. 电网技术, 2020, 44(2): 530 – 538.)
- [19] ZHAO Shuqiang, WANG Hui, TIAN Na, et al. Model Predictive Control Based DC Microgrid Virtual Inertia Optimal Method. *Transactions of China Electrotechnical Society*, 2023, 38(12): 3264 – 3276.
(赵书强, 王慧, 田娜, 等. 基于模型预测控制的直流微电网虚拟惯量优化方法. 电工技术学报, 2023, 38(12): 3264 – 3276.)
- [20] ZHANG Haikuo, MENG Xiuqun. UAV online path planning of based on improved RRT algorithm. *Systems Engineering and Electronics*, 2024, 6: 1 – 10.
(张海阔, 孟秀云. 基于改进RRT算法的无人机在线航迹规划. 系统工程与电子技术, 2024, 6: 1 – 10.)
- [21] YE Lin, LU Peng, ZHAO Yongning, et al. Review of Model Predictive Control for Power System With Large-scale Wind Power Grid-connected. *Proceedings of the CSEE*, 2021, 41(18): 6181 – 6197.
(叶林, 路朋, 赵永宁, 等. 含风电电力系统有功功率模型预测控制方法综述. 中国电机工程学报, 2021, 41(18): 6181 – 6197.)
- [22] YUAN C, ZHAO D, HEIDARI A A, et al. Artemisinin optimization based on malaria therapy: Algorithm and applications to medical image segmentation. *Displays*, 2024, 5: 1 – 64.
- [23] LI B, YANG R, XU D, et al. Analysis of the phase-shifted carrier modulation for modular multilevel converters. *IEEE Transactions on Power Electronics*, 2015, 30 (1): 297 – 310.
- [24] LYU Xin, MU Xiaodong, ZHANG Jun, et al. Chaos sparrow search optimization algorithm. *Journal of Beijing University of Aeronautics and Astronautics*, 2021, 47(8): 1712 – 1720.
(吕鑫, 慕晓冬, 张钧, 等. 混沌麻雀搜索优化算法. 北京航空航天大学学报, 2021, 47(8): 1712 – 1720.)
- [25] SHAN Liang, QIANG Hao, LI Jun, et al. Chaotic optimization algorithm based on Tent map. *Control and Decision*, 2005, 20(2): 179 – 182.
(单梁, 强浩, 李军, 等. 基于Tent映射的混沌优化算法. 控制与决策, 2005, 20(2): 179 – 182.)

作者简介:

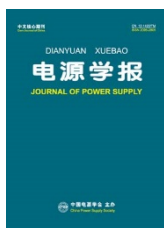
李锦键 博士研究生, 研究方向为可再生能源发电系统与控制, 微电网技术, E-mail: lijnjian0326@163.com;

王兴贵 教授, 博士生导师, 研究方向为可再生能源发电系统与控制, 微电网技术, 电力电子与电力传动等, E-mail: wangxg8201@163.com;

李昱 硕士研究生, 研究方向为可再生能源发电系统与控制, E-mail: liyu6968266@163.com;

丁颖杰 博士研究生, 研究方向为可再生能源发电系统与控制, 微电网技术, E-mail: dingyj0820@126.com;

薛晟 博士, 副教授, 硕士生导师, 研究方向为可再生能源发电系统与控制, 微电网技术, E-mail: xueshenglut@126.com;



电源学报
Journal of Power Supply
ISSN 2095-2805, CN 12-1420/TM

《电源学报》网络首发论文

题目: 基于改进 PPO 的 HCSY-MG 并网系统分布式混合储能充放电优化控制
作者: 李锦键, 王兴贵, 丁颖杰
收稿日期: 2024-08-14
网络首发日期: 2024-10-25
引用格式: 李锦键, 王兴贵, 丁颖杰. 基于改进 PPO 的 HCSY-MG 并网系统分布式混合储能充放电优化控制[J/OL]. 电源学报.
<https://link.cnki.net/urlid/12.1420.TM.20241025.1052.002>



网络首发: 在编辑部工作流程中, 稿件从录用到出版要经历录用定稿、排版定稿、整期汇编定稿等阶段。录用定稿指内容已经确定, 且通过同行评议、主编终审同意刊用的稿件。排版定稿指录用定稿按照期刊特定版式 (包括网络呈现版式) 排版后的稿件, 可暂不确定出版年、卷、期和页码。整期汇编定稿指出版年、卷、期、页码均已确定的印刷或数字出版的整期汇编稿件。录用定稿网络首发稿件内容必须符合《出版管理条例》和《期刊出版管理规定》的有关规定; 学术研究成果具有创新性、科学性和先进性, 符合编辑部对刊文的录用要求, 不存在学术不端行为及其他侵权行为; 稿件内容应基本符合国家有关书刊编辑、出版的技术标准, 正确使用和统一规范语言文字、符号、数字、外文字母、法定计量单位及地图标注等。为确保录用定稿网络首发的严肃性, 录用定稿一经发布, 不得修改论文题目、作者、机构名称和学术内容, 只可基于编辑规范进行少量文字的修改。

出版确认: 纸质期刊编辑部通过与《中国学术期刊 (光盘版)》电子杂志社有限公司签约, 在《中国学术期刊 (网络版)》出版传播平台上创办与纸质期刊内容一致的网络版, 以单篇或整期出版形式, 在印刷出版之前刊发论文的录用定稿、排版定稿、整期汇编定稿。因为《中国学术期刊 (网络版)》是国家新闻出版广电总局批准的网络连续型出版物 (ISSN 2096-4188, CN 11-6037/Z), 所以签约期刊的网络版上网络首发论文视为正式出版。

基于改进 PPO 的 HCSY-MG 并网系统分布式混合储能 充放电优化控制

李锦键（中国电源学会学生会员），王兴贵，丁颖杰（中国电源学会学生会员）

（兰州理工大学电气工程与信息工程学院，兰州 730050）

摘要：为平抑微源半桥变流器串联星型结构微电网(half-bridge converter series Y-connection microgrids, HCSY-MG)并网系统中微源出力的波动，保证各相直流侧电压之和相等与并网电流三相平衡，提出一种基于改进近端策略优化(proximal policy optimization, PPO)的分布式混合储能(hybrid energy storage system, HESS)充放电优化控制策略。在考虑 HCSY-MG 系统并网电流与分布式 HESS 特性的条件下，确定了影响并网电流的主要系统变量，以及 HESS 接入系统的最佳拓扑结构。然后结合串联系统的特点，将分布式 HESS 的充放电问题转换为深度强化学习的 Markov 决策过程。同时针对 PPO 算法中熵损失权重难以确定的问题，提出一种改进的 PPO 算法，兼顾了智能体的收敛性和探索性。最后以某新能源发电基地的典型运行数据为算例，验证本文所提控制策略的可行性和有效性。

关键词：串联微电网；分布式混合储能；近端策略优化；充放电功率；深度强化学习

Optimal Control of Distributed Hybrid Energy Storage Charge-discharge for HCSY-MG Grid-connected System Based on Improved PPO

LI Jinjian, *Student Member, CPSS*, WANG Xinggui, DING Yingjie, *Student Member, CPSS*

(School of Electrical Engineering and Information Engineering, Lanzhou University of Technology, Lanzhou 730050, China)

Abstract: To mitigate fluctuations in the output of micro-sources within half-bridge converter series Y-connection microgrid (HCSY-MG) grid-connected system and to ensure both the balance of the sum of DC-side voltages and the 3-phase grid-connected current, a distributed hybrid energy storage system (HESS) charge-discharge optimization control method based on the improved proximal policy optimization (PPO) is proposed. Taking into account the grid-connected current of the HCSY-MG system and the characteristics of the distributed HESS, the key system variables affecting the grid-connected current are identified, and the optimal topology for integrating the HESS into the system is determined. Subsequently, considering the characteristics of the series-connected system, the charge-discharge problem of the distributed HESS is transformed into a Markov

收稿日期：2024-08-14；修回日期：2024-09-18；录用日期：2024-10-07

基金项目：国家自然科学基金项目(基金编号 51967011)

This work is supported by the National Natural Science Foundation of China under the grant 51967011

decision process within the framework of deep reinforcement learning. To address the challenge of determining the entropy loss weight in the PPO method, an improved PPO approach is proposed, which balances the agent's convergence and exploration capabilities. Finally, using typical operational data from a renewable energy generation site as a case study, the proposed control strategy is validated as both feasible and effective in a series-connected microgrid.

Keywords: Series-connected microgrid; distributed hybrid energy storage; proximal policy optimization; charge-discharge power; deep reinforcement learning

引言

在传统交流微电网中, 可再生能源发电单元与负载大都通过电力电子变流器并联在交流母线上。该拓扑结构导致传统交流微电网中存在着诸如环流和谐波抑制困难, 控制复杂等问题。针对交流微电网目前存在的问题, 文献[1]提出一种半桥变流器串联星型结构微电网(half-bridge converter series Y-connection microgrids, HCSY-MG)系统。HCSY-MG系统凭借串联特性, 从拓扑结构上解决了传统交流微电网中存在的问题, 同时使系统的控制更为简单。在 HCSY-MG 系统中, 为补偿可再生能源发电固有的波动性, 会在各发电单元(generator module, GM)直流侧并联混合储能系统(hybrid energy storage system, HESS)。因为 HESS 分布在各 GM 直流侧, 所以该种储能方式也被称为分布式储能。与集中式储能相比, 分布式储能可以根据不同微源的特性, 更有针对性地采取相应的控制策略, 并且在协调控制时能达到更优的效果。与传统 H 桥链式结构组成的微电网相比, HCSY-MG 系统在微源数量一定的条件下, 所使用的开关器件数量减半, 可显著降低微电网系统的投资成本, 同时半桥变流器的控制也更加简单、灵活^[1]。但 HCSY-MG 系统仍旧存在例如可再生能源波动造成输出电压电流中含有部分直流和 50Hz 低频脉动分量, 以及分布式 HESS 投资成本会不可避免上升等问题。为解决可再生能源波动性造成的以上问题, 研究人员广泛采用优化 HESS 充放电功率的方法。但在串联型微电网中, 仅有部分关于串联型微电网中分布式 HESS 单体控制策略的研究, 结合串联系统特点的 HESS 充放电功率协调优化控制却鲜有研究。所以, 本文将研究一种 HCSY-MG 并网系统中分布式 HESS 的充放电控制策略, 在充分利用系统特点和优势的基础上, 降低可再生能源发电波动性对系统的不利影响。

微电网中储能系统的充放电优化控制可以描述为考虑多种因素变化时的充放电功率或状态的时序安排, 即序贯决策问题^[2]。为解决序贯决策问题, 目前广泛采用的方法包括经典优化方法、基于规划的方法、启发式优化方法和深度强化学习(deep reinforcement learning, DRL)方法等^[3]。其中, DRL 凭借着能够利用微电网大量数据, 根据不同运行要求和优化目标, 在实时决策的同时给出相应的控制方案和优化策略, 已经成为当下的一个研究热点。针对不同的控制目

标, 目前已有 DRL 中的多种算法被应用至微电网储能装置的调度与控制。文献[4]考虑了可再生能源出力的未来不确定性, 利用双重深度 Q 学习算法对微电网中储能装置进行调度, 成功降低了微电网的运行成本。文献[5]在考虑多种其他因素的基础上, 在通过双重深度 Q 学习方法降低微电网运行成本的同时, 与启发式方法对比, 并说明了 DRL 方法的可行性和优越性。文献[6]利用深度确定性策略梯度方法对微电网中的储能进行控制, 实现了运行利润的最大化。除考虑微电网运行的经济性以外, 文献[7-8]分别从最小化网损和储能系统功率损耗两方面出发, 利用近端策略优化 (proximal policy optimization, PPO) 方法和 Q-学习方法对微电网中的能量调度进行优化。文献[9]提出了一种两步超前的储能调度 DRL 方法, 提高了储能和可再生能源的利用率。文献[10]利用柔性策略评价算法控制微电网中储能的充放电, 使微电网中的电压偏移最小。在 DRL 方法中, 基于策略梯度的算法通过构建策略网络, 避免了对动作的离散化, 使相应算法能够应用至连续动作空间的环境中^[11]。针对传统策略梯度算法对步长的选择较为敏感的问题, 文献[12]为提高算法稳定性和对超参数的鲁棒性, 提出了置信域策略优化算法, 避免了策略参数发生大范围变化, 但该算法的计算效率较低。文献[13]在置信域策略优化算法的基础上提出了一种基于剪切函数的 PPO 算法, 通过多个训练回合对参数进行小批量更新, 在提高算法计算效率的同时, 保留了置信域策略优化算法的优点。

本文在确定适用于 HCSY-MG 并网系统 HESS 拓扑结构的基础上, 充分考虑串联型微电网的特性, 以各相直流侧电压之和偏差最小为目标, 提出一种基于改进 PPO 算法的 HESS 充放电功率优化控制策略。同时根据训练过程中损失函数的变化, 提出一种改进的 PPO 算法, 使熵损失函数中的权重因子自适应更新, 解决了熵损失权重难以确定的问题。并以某新能源发电基地的典型运行数据为算例, 对所提方法的可行性和有效性进行验证。

1 HCSY-MG 并网系统

1.1 HCSY-MG 系统结构

HCSY-MG 系统的拓扑结构如图 1 所示。在该系统中, 每相均由 N 个 GM 串联组成, 并以星型连接的方式组成三相逆变环节, 然后经滤波器、变压器等装置连接于交流母线。

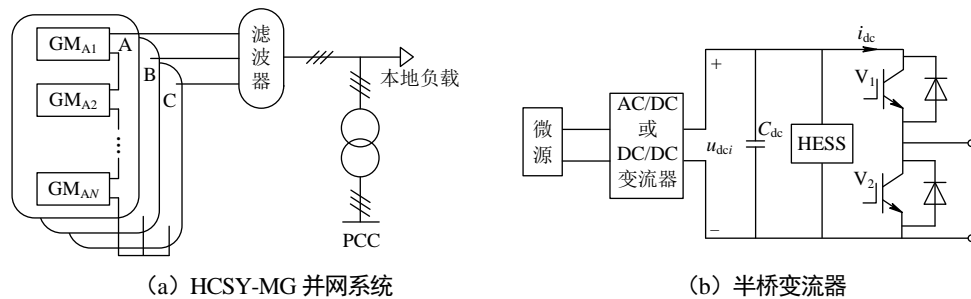


图 1 HCSY-MG 系统拓扑结构

Fig. 1 Topology structure of HCSY-MG system

由图 1(b)可以看出, 每个 GM 由微源、AC/DC 或 DC/DC 变流器、稳压电容 C_{dc} 、HESS 和半桥变流器组成。为便于分析, 将每个 GM 等效为受控电压源, 则可得到 HCSY-MG 并网系统的等效电路如图 2 所示。图中, u_{xO} 为三相逆变环节输出电压; R_e 为线路等效电阻; i_x 为系统输出电流; u_{xN} 为等效单相输出电压; i_{Lx} 为负载电流; i_{ex} 为并网电流; e_x 为电网电压。其中, $x=A、B、C$ 。

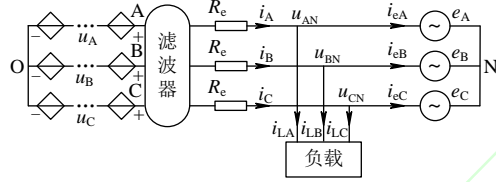


图 2 HCSY-MG 并网系统等效电路

Fig. 2 Equivalent circuit of the grid-connected HCSY-MG system

1.2 HCSY-MG 系统并网电流模型

由图 2 可得 HCSY-MG 等效单相并网系统的 KVL 方程为:

$$u_{xN} = L_f \frac{di_x}{dt} + R_e i_x + e_x \quad (1)$$

进一步, 令 $i_{ex} = i_x - i_{Lx}$, 可得到三相并网电流的矩阵表达式为:

$$L_f \frac{d}{dt} \begin{bmatrix} i_{eA} \\ i_{eB} \\ i_{eC} \end{bmatrix} + \begin{bmatrix} R_e & 0 & 0 \\ 0 & R_e & 0 \\ 0 & 0 & R_e \end{bmatrix} \begin{bmatrix} i_{eA} \\ i_{eB} \\ i_{eC} \end{bmatrix} = \begin{bmatrix} u_{AN} - e_{AN'} \\ u_{BN} - e_{BN'} \\ u_{CN} - e_{CN'} \end{bmatrix} \quad (2)$$

式中, u_{AN} 、 u_{BN} 、 u_{CN} 的表达式分别为^[14]:

$$u_{AN} = \frac{2u_{AO} - u_{BO} - u_{CO}}{3} = \frac{1}{3} \left[(u_{dcA} - \frac{1}{2}u_{dcB} - \frac{1}{2}u_{dcC}) + \frac{\sqrt{3}}{4}M(u_{dcB} - u_{dcC})\cos\omega_0 t + \frac{M}{4}(4u_{dcA} + u_{dcB} + u_{dcC})\sin\omega_0 t \right];$$

$$u_{BN} = \frac{2u_{BO} - u_{AO} - u_{CO}}{3} = \frac{1}{3} \left[(u_{dcB} - \frac{1}{2}u_{dcA} - \frac{1}{2}u_{dcC}) - \frac{\sqrt{3}}{4}M(2u_{dcB} + u_{dcC})\cos\omega_0 t - \frac{M}{4}(2u_{dcA} + 2u_{dcB} - u_{dcC})\sin\omega_0 t \right];$$

$$u_{CN} = \frac{2u_{CO} - u_{AO} - u_{BO}}{3} = \frac{1}{3} \left[(u_{dcC} - \frac{1}{2}u_{dcA} - \frac{1}{2}u_{dcB}) + \frac{\sqrt{3}}{4}M(u_{dcB} + 2u_{dcC})\cos\omega_0 t - \frac{M}{4}(2u_{dcA} - u_{dcB} + 2u_{dcC})\sin\omega_0 t \right];$$

其中, $u_{dcx} = \sum_{i=1}^N u_{dcx}(i)$ 为逆变侧 x 相 GM 直流侧电压之和; M 为调制比; ω 为调制波角频率。

由上式所表示的 HCSY-MG 系统并网电流数学模型可以看出, 若各相 GM 直流侧电压之和存在偏差导致不相等时, 会造成系统输出电压中产生直流分量和基频偏差量, 进而会使得并网电流中同样存在直流分量和基频偏差量。所以, 在可再生能源发电存在波动的条件下, 通过对 HCSY-MG 系统中分布式 HESS 的充放电功率进行优化控制, 可以保证系统各相 GM 直流侧电压之和保持一致, 从而降低并网电流中的直流分量和基频偏差量。

根据以上对 HCSY-MG 系统并网电流数学模型的分析, 为降低可再生能源发电波动性对并网电流的影响, 在结合

系统串联特性的基础上，对系统中分布式 HESS 的充放电功率进行优化控制是十分必要的。

2 含有 HESS 的 GM 内部功率特性分析

目前，HESS 接入微电网直流侧的拓扑结构主要有 4 种，分别为蓄电池和超级电容均通过双向 DC/DC 变流器接入 GM 直流侧，仅蓄电池通过双向 DC/DC 变流器接入，仅超级电容通过双向 DC/DC 变流器接入，蓄电池和超级电容均直接接入。考虑到超级电容和蓄电池的响应时间，以及功率开关器件和控制系统的动作时间，若超级电容通过双向 DC/DC 变流器接入 GM 直流侧，不仅会增大系统的控制成本，而且可能会影响 HESS 对 GM 高频功率波动的抑制效果；而蓄电池一般用于抑制 GM 的低频功率波动，为保证抑制效果，则必须通过双向 DC/DC 变流器将蓄电池接入 HESS。同时，因为超级电容的本质为电容器，所以本文将 GM 内部的稳压电容直接替换为 HESS 中的超级电容，同时承担稳定 GM 直流母线电压和平抑高频功率波动的任务。

综上，本文所采用的 HESS 拓扑结构及其内部功率流动情况如图 3 所示。图中， P_M 为微源输出功率； P_C 为超级电容充放电功率； P_B 为蓄电池充放电功率； P_G 为 GM 输出功率。

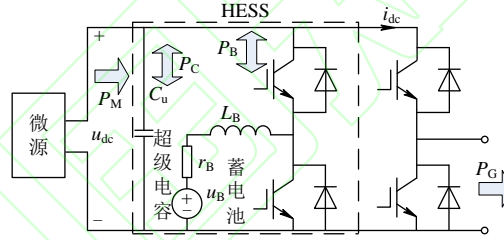


图 3 GM 内部功率流动情况

Fig. 3 Internal power flow within the GM

当 GM 正常工作时，其内部功率满足：

$$P_M - P_C - P_B = P_G \quad (3)$$

其中， P_C 的表达式为：

$$P_C = u_{dc} C_u \frac{du_{dc}}{dt} \quad (4)$$

由式(4)可看出，当 GM 直流侧电压 u_{dc} 保持恒定时， $P_C=0$ 。此时，GM 内部的功率满足：

$$P_B = P_M - P_G = \Delta P_{GM} \quad (5)$$

由以上 GM 内部功率流动情况可以看出，当 GM 内部功率流动保持平衡时，GM 直流母线的电压也将保持稳定，所以需要利用 HESS 平抑微源输出功率的波动，以保证 GM 直流侧电压的稳定。

结合上文对 GM 内部功率流动的分析，以及本文所采用的 HESS 拓扑结构，下文将使用 DRL 方法中的改进 PPO 算法对 HCSY-MG 并网系统中各 GM 直流侧的 HESS 充放电功率进行优化控制，以保证系统各相直流侧电压之和稳定，

降低可再生能源波动性对并网电流的不利影响。

3 基于改进 PPO 的 HESS 充放电功率优化

3.1 强化学习问题建模

DRL 一般可以描述为马尔科夫决策过程(Markov decision process, MDP)。传统的 MDP 包含有 4 要素, 由 (S, A, R, π) 组成的四元数组给出。其中 S 为环境状态集合, A 为智能体采取的动作集合, R 为智能体采取某种动作的奖惩函数, π 为在某种状态下选择动作的策略^[15]。结合 HCSY-MG 并网系统的特点, 以上各部分可以描述为:

①环境状态集合 S 。环境状态集合由智能体需要感知的环境状态变量组成, 即环境需要给智能体提供的信息, 包括: 每一个微源的实际出力 P_{xi} 、每一相 GM 直流侧电压之和 u_{dcx} 、每一个 GM 直流侧 HESS 中蓄电池的 SOC_{xi} 、三相并网电流的总谐波畸变率 THD_x 。所以, 环境状态集合 S 可以表示为:

$$S = [P_{xi}(t), u_{dcx}(t), SOC_{xi}(t), THD_x] \quad (6)$$

式中, $x=A, B, C$, 表示三相; $i=1, 2, \dots, N$ 。

②动作空间 A 。动作空间是智能体在获得环境的状态信息后, 可能采取动作的集合。因为本文的目的是 HCSY-MG 并网系统中分布式 HESS 充放电功率的优化控制, 所以动作空间定义为各 GM 中蓄电池的充放电功率, 即:

$$A = [P_{B_xi}(t)] \quad (7)$$

式中, $P_{B_xi}(t)$ 为蓄电池的充放电功率。

③奖惩函数 R 。奖惩函数是环境对当前动作的即时回报, 直接影响着智能体对动作的选择。本文所选择的奖惩函数由正向奖励和反向惩罚两部分组成, 当各相直流侧电压之和的偏差在允许范围内时, 给予奖励; 当 HCSY-MG 并网系统的状态越限时, 给予惩罚。所以, 本文选择的奖惩函数 R 可以表示为:

$$R = 100 \left\{ \Delta u_{dcx} \leq \Delta u_{dc}^{\max} \right\} - 10 \left\{ \Delta u_{dcx} > \Delta u_{dc}^{\max} \right\} - 10 \left\{ P_{B_xi}(t) < P_{B_xi}^{\min}, P_{B_xi}(t) > P_{B_xi}^{\max} \right\} - 10 \left\{ SOC_{B_xi}(t) < SOC_{B_xi}^{\min}, SOC_{B_xi}(t) > SOC_{B_xi}^{\max} \right\} - 10 \{ \text{change} \} - 100 \{ THD_x \geq 5\% \} \quad (8)$$

式中, Δu_{dc}^{\max} 为各相直流侧电压之和偏差的最大允许范围; $P_{B_xi}^{\min}$ 与 $P_{B_xi}^{\max}$ 分别为蓄电池的最小与最大充放电功率; $SOC_{B_xi}^{\min}$ 与 $SOC_{B_xi}^{\max}$ 分别为蓄电池 SOC 的最小与最大值; change 表示更换充放电的 GM, 为提高储能的使用寿命, 避免频繁启停, 故此时给予一个较小的惩罚系数; 当并网电流 $THD_x \geq 5\%$ 时, 将不满足 IEEE 关于并网电流 THD 的要求, 故此时给予一个较大的惩罚系数。

④动作选择策略 π 。动作选择策略是指智能体在当前环境条件下选择动作的策略。在本文中, 动作选择策略由 PPO 算法给出, 一般 PPO 算法由策略网络、策略网络副本和价值网络组成, 所以下文将对 PPO 算法进行详细说明。

3.2 改进的近端策略优化算法

根据上一小节中关于动作选择策略 π 的叙述,本文选用PPO算法求解动作选择策略。PPO算法具有3个网络,分别为策略网络、策略网络副本、价值网络,各网络的作用分别为^[16]:①策略网络(Actor网络)。策略网络的输入为状态空间 S ,输出为动作空间 A 。该网络可根据经验回放池中的数据,多次更新网络参数 θ 。②策略网络副本(Actor网络副本)。策略网络副本则与策略网络相同,负责与环境交互,将获得小批量数据 (S, A, R) 存入经验回放池。策略网络副本的参数 θ_{old} 定期从 θ 复制。③价值网络(Critic网络)。价值网络的输入为状态空间 S 和动作空间 A ,输出则为价值函数。该网络可根据环境当前状态,评估状态价值,估计优势函数。

PPO算法的目标函数 $L_t(\theta)$ 可以表示为^[13]:

$$L_t(\theta) = \hat{E}_t \left[L_t^{CLIP}(\theta) - c_1 L_t^{VF}(\theta) + \omega S[\pi_\theta](s_t) \right] \quad (9)$$

式中, c_1 为平方误差系数; ω 为熵损失系数; $L_t^{CLIP}(\theta) = \hat{E}_t \left[\min \left(\frac{\pi_\theta(a_t|s_t)}{\pi_{\theta_{old}}(a_t|s_t)} \hat{A}_t, \text{clip} \left(\frac{\pi_\theta(a_t|s_t)}{\pi_{\theta_{old}}(a_t|s_t)}, 1-\epsilon, 1+\epsilon \right) \hat{A}_t \right) \right]$, 其

中 $\hat{A}_t = \delta_t + (\gamma\lambda)\delta_{t+1} + \dots + (\gamma\lambda)^{T-t+1}\delta_{T-1}$, $\delta_t = r_t + \gamma V(s_{t+1}) - V(s_t)$; $L_t^{VF}(\theta) = [V(s_t) - G(t)]^2$ 为平方误差损失, 其

中 $G(t) = r_{t+1} + \gamma r_{t+2} + \dots + \gamma^{T-t} r_{T+1} + \gamma^{T-t+1} v(s_{T+1})$; $S[\pi_\theta] = \frac{1}{2} \sum_{k=1}^c \ln(2\pi \cdot e \cdot \sigma_{k,i}^2)$ 为熵损失。

在式(9)中,熵损失系数 ω 作为一个关键参数,影响着智能体对于动作的更新。当熵损失系数 ω 过高时,智能体动作的不确定性会增高,从而进行更多探索,帮助智能体更快跳出局部最优;当熵损失系数 ω 过低时,智能体动作的不确定性会减弱,易陷入局部最优,导致最终不能收敛至最优结果。所以,为解决熵损失系数难以确定的问题,本文将利用自适应思想,使熵损失系数在训练过程中自适应更新,以在寻优过程中兼顾收敛性和探索性。

在改进策略中,通过比较当前训练回合中目标函数值与已执行训练回合平均目标函数值的大小,决定熵损失系数在下一轮训练回合中的大小,即:

$$\omega = \begin{cases} \omega_{\max}, & \text{other} \\ \omega_{\min} + \frac{(L_t(\theta) - L_{\min}(\theta))(\omega_{\max} - \omega_{\min})}{L_{\text{ave}}(\theta) - L_{\min}(\theta)}, & L_t(\theta) < L_{\text{ave}}(\theta) \end{cases} \quad (10)$$

式中, ω_{\min} 与 ω_{\max} 分别为熵损失系数的最小与最大值; $L_{\min}(\theta)$ 为已执行训练回合中目标函数的最小值; $L_{\text{ave}}(\theta)$ 为已执行训练回合中目标函数的平均值。

根据以上关于改进PPO算法的叙述,可以得到该算法的流程如表1所示。

表 1 改进 PPO 算法的流程

Tab. 1 The flow of the improved PPO algorithm

| 改进 PPO 算法 |
|---|
| 输入: Actor 网络 (参数为 θ) , Actor 网络副本 (参数为 θ_{old}) , Critic 网络 (参数为 ω) , 训练次数 n , 每一轮训练网络的更新次数 K ; |
| 输出: Actor 网络 (参数为 θ) , Critic 网络 (参数为 ω) ; |
| 过程: 初始化 θ , ω , $\theta_{old}=\theta$, 经验回放集合 D ; |
| for $i=1,2,\dots,n$ |
| Actor 网络副本与环境交互 T 步, 将每步得到的 (S_t, A_t, R_t, S_{t+1}) 放入经验回放集合 D ; |
| for $k=1,2,\dots,K$ |
| if $\text{length}(D)\geq\text{batch_size}$ |
| Critic 网络评估状态价值 V_1, V_2, \dots, V_T , 并估计优势函数 $\hat{A}_1, \hat{A}_2, \dots, \hat{A}_T$; |
| end if |
| 计算目标函数, 更新策略网络和价值网络, 并根据式(10)更新熵损失系数; |
| end for |
| $\theta \leftarrow \theta_{old}$, 并初始化经验回放集合 D ; |
| end for |

4 算例分析

4.1 算例基本参数与数据

算例所使用的数据来自于某新能源发电基地的典型运行数据, 其他主要参数如表 2 所示。

表 2 算例中主要参数

Tab. 2 The main parameters in the example

| 环境参数 | | 改进 PPO 参数 | | | |
|-------------|--------------------------|-----------|----------------------|--------------|-------------------------|
| 参数 | 数值 | 参数 | 数值 | 参数 | 数值 |
| 串联 GM 数量 | $N=4$ | 平方误差系数 | $c_1=0.05$ | 剪切系数 | $\varepsilon=0.2$ |
| GM 直流侧电压 | $u_{dk}=160\text{V}$ | 熵损失系数最小值 | $\omega_{\min}=0.8$ | 经验回放集合容量 | $\text{length}(D)=1000$ |
| 蓄电池 SOC 最小值 | $\text{SOC}_{\min}=20\%$ | 熵损失系数最大值 | $\omega_{\max}=0.01$ | Actor 网络学习率 | 0.0001 |
| 蓄电池 SOC 最大值 | $\text{SOC}_{\max}=80\%$ | 训练次数 | $n=800$ | Critic 网络学习率 | 0.0005 |
| 蓄电池充放电功率最大值 | $P_B^{\max}=1\text{kW}$ | 每轮更新频率 | $k=10$ | | |

Actor 网络与 Actor 网络副本的结构是相同的, 并且输入为状态空间 S , 所以输入层的神经元数量为 30; 输出为相应的动作 a_t , 所以输出层的神经元数量为 1; 隐含层设置为 2 层, 每层分别由 60 和 128 个神经元组成, 隐含层激活函数选择为 ReLu。Critic 网络的输入则为状态和动作, 所以输入层和输出层的神经元数量分别为 31 与 1, 隐含层及其激活函数与 Actor 网络设置相同。本文所采用的改进 PPO 算法的神经网络结构图如图 4 所示。

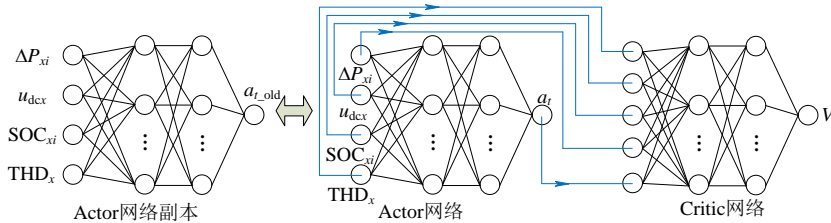


图 4 神经网络结构图

Fig. 4 Neural network architecture

4.2 训练过程

在训练过程中, 设置每一相微源的组成为: 风电、风电、光伏、光伏, 并以 A 相为例进行算例分析。为突出 HCSY-MG 系统串联的特点, 假设 A 相中第一个风电微源和第三个光伏微源的出力出现如图 5 所示的波动。

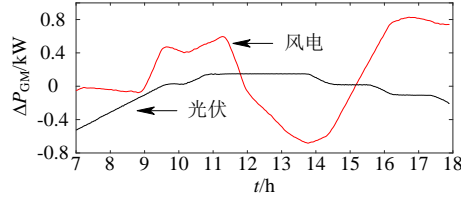


图 5 风电和光伏微源的功率波动曲线

Fig. 5 Power fluctuation curves for wind and PV microsources

在该种工况下, A 相中的微源出力出现波动, GM 直流侧电压之和也将出现波动; 而 B、C 相中的微源出力稳定, GM 直流侧电压之和稳定在 640V。同时设置相应 GM 中蓄电池的 SOC 初始值分别为 60%, 60%, 40%, 40%; 风电和光伏 GM 中蓄电池的容量分别为 3 和 2kW·h^[17]。在训练过程中, 采用传统 PPO 算法与采用本文所提改进 PPO 算法的平均奖励函数曲线如图 6 所示。

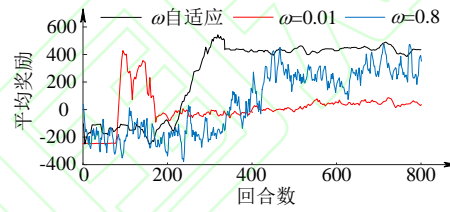


图 6 训练过程中的奖励函数曲线

Fig. 6 Reward function curves during training

由图 6 中的奖励函数曲线可以看出, 当熵损失系数 $\omega=0.01$ 时, 尽管在训练的初始阶段可以获得奖励较大的动作, 但会陷入局部最优, 并且由于智能体探索能力不足, 在陷入局部最优时不能快速地跳出, 导致达到最大训练回合数的时候无法学得奖励最大的动作。当熵损失系数 $\omega=0.8$ 时, 平均奖励曲线波动剧烈, 说明此时智能体的搜索能力较强, 可以充分探索动作空间, 但在训练后期存在着不易收敛的特点。当熵损失系数 ω 按照本文所提出的自适应策略进行更新时, 在训练初始阶段可以较快地学得奖励较大的动作, 并且在达到最大训练回合数时, 收敛效果较好。以上关于训练过程中奖励函数曲线的分析与 3.2 小节关于熵损失系数 ω 的理论分析基本一致, 也证明了本文所提出的熵损失系数自适应更新策略可以在保证 PPO 算法收敛性的同时兼顾探索性。

4.3 测试结果

在所设置的环境条件下, 利用具有奖励函数值较高的动作与环境进行交互测试, 得到 A 相 4 个 GM 中蓄电池的充放电功率 P_B 曲线、对应的 SOC 曲线和直流侧电压曲线如图 7 所示。

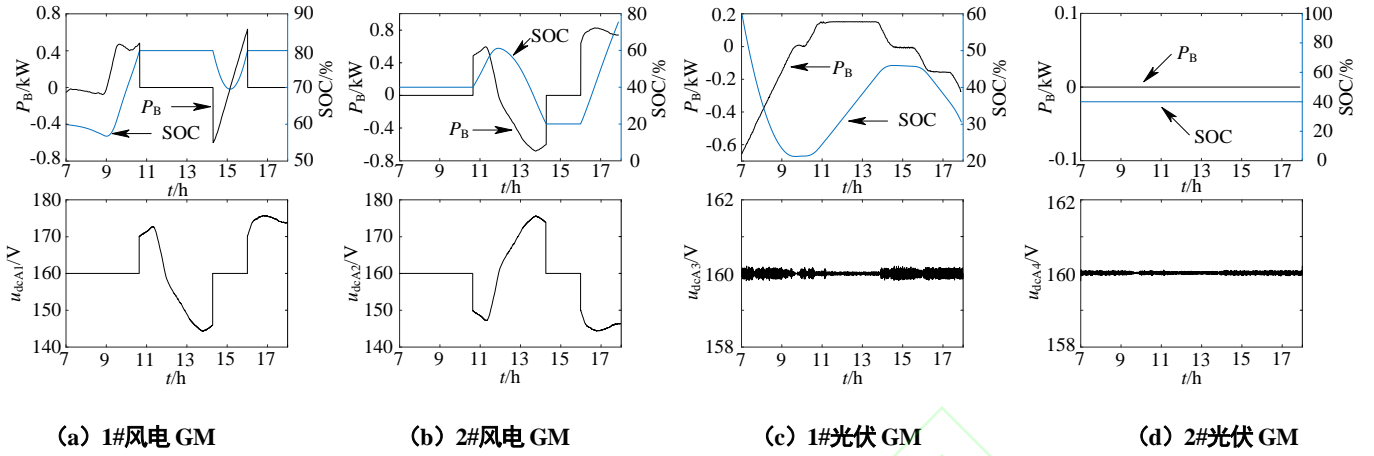


图 7 HESS 中蓄电池的充放电功率及其 SOC 曲线
Fig. 7 Charge-discharge power of batteries in HESS and their SOC curves

由图 7 中的 HESS 充放电功率曲线可以看出，A 相中各 GM 中的蓄电池充放电功率均未超过最大值 1kW，同时对应的 SOC 均在[20%, 80%]的规定区间内，说明智能体得出的最优动作满足相应约束条件。在大约 10.5h 时，1#风电 GM 中的蓄电池充电至 SOC=80%；因为要继续维持吸收能量的状态，所以此时 A 相中 SOC 最低，剩余容量最多的 2#风电 GM 中的蓄电池开始充电；在大约 14.5h 时，2#风电 GM 中的蓄电池放电至 SOC=20%，因为要继续维持释放能量的状态，所以此时 A 相中 SOC 最高，储存能量最多的 1#风电 GM 中的蓄电池开始放电。关于 1#光伏 GM 直流侧功率发生波动时，由于波动范围较小，且式(8)中更换充放电模块的惩罚项，所以在满足相应约束条件的情况下，该模块的功率波动由该模块自身的蓄电池进行平抑。同时，结合 A 相中各 GM 的直流侧电压曲线可以看出，本文提出的 HESS 充放电优化控制可以较好结合 HCSY-MG 并网系统的特点，协调控制各 GM 中配备的 HESS 系统。在 1#风电 GM 中蓄电池 SOC 超过允许值时，结合 HCSY-MG 并网系统的特点，在本文所提 HESS 充放电优化控制方法下，利用 2#风电 GM 中的蓄电池平抑可再生能源波动对系统直流侧电压之和，以及对并网电流的影响。若不结合 HCSY-MG 并网系统的特点，单独利用各 GM 中配备的 HESS 对其可再生能源出力波动进行平抑，本文所设定的蓄电池容量无法满足平抑需求。在此条件下，若要利用 HESS 对可再生能源出力波动的平抑，以减轻对系统直流侧电压之和，以及对并网电流的影响，则蓄电池的容量势必要增加，从而会增加相应的投资成本。所以，本文在考虑 HCSY-MG 并网系统特点的条件下，提出的 HESS 充放电功率优化控制方法可以使得 HESS 的容量保持在一个较低的范围，从而降低 HESS 的投资成本。

A 相各 GM 直流侧 HESS 中的蓄电池直接接入（即不对其充放电功率进行控制）时，以及采用本文所提充放电功率优化控制策略条件下，HCSY-MG 并网系统的 A 相 GM 直流侧电压之和的曲线，以及三相并网电流的曲线如图 8 和图 9 所示。

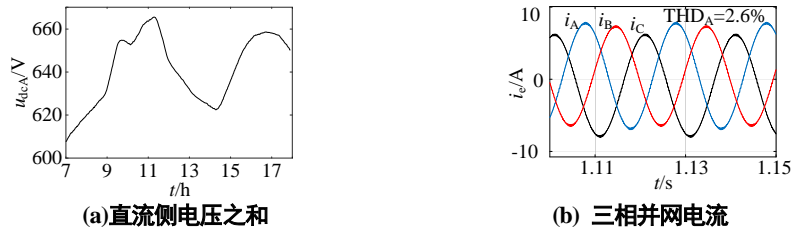


图 8 蓄电池直接接入 GM 直流侧时的系统特征

Fig. 8 System characteristics when the battery directly connected to the DC side of GM

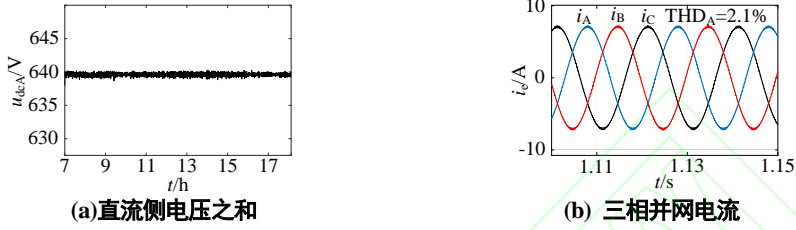


图 9 蓄电池采用本文所提控制策略时的系统特征

Fig. 9 System characteristics when the battery apply the control strategy proposed in this paper

由图 8(a)可以看出, HESS 中蓄电池直接接入 GM 直流侧的方法不能完全平抑可再生能源出力的波动性, A 相直流侧电压之和仍存在着波动。当 $u_{dcA}=610V$ 时, 三相并网电流的曲线如图 8(b)所示, 此时三相并网电流中分别含有-1A、0.5A 和 0.3A 的直流分量, 并且 A 相并网电流的 $THD_A=2.6\%$ 。当 HESS 中蓄电池的充放电功率采用本文所提控制策略时, A 相直流侧电压之和仅在一个小范围内波动。相同时间点的三相并网电流曲线如图 9(b)所示, 此时三相并网电流中的直流分量分别为-0.02A、0.01A 和 0.004A, 均下降了约 98%, 并且 A 相并网电流的 THD 降低至 2.1%。该结果证明本文所提出的 HESS 充放电功率控制策略能够有效降低可再生能源波动对 HCSY-MG 系统直流侧电压之和, 以及对并网电流的不利影响。

以上测试结果证明了本文所提基于改进 PPO 算法的 HCSY-MG 并网系统分布式 HESS 充放电优化控制策略是可行的、有效的, 且具有一定的经济价值。

5 结论

针对 HCSY-MG 并网系统中微源出力波动造成各相 GM 直流侧电压之和不相等, 进一步会对并网电流造成不利影响的问题, 本文在确定影响 HCSY-MG 系统并网电流的主要变量, 以及适用于该微电网 HESS 拓扑结构的基础上, 提出一种基于改进 PPO 算法的分布式 HESS 充放电功率优化控制策略。同时, 为降低熵损失系数设置对智能体动作选择的影响, 提出一种熵损失自适应更新的改进 PPO 算法。本文所提出的 HCSY-MG 并网系统 HESS 充放电控制方法能够充分发挥系统的特点和优势, 不仅可以在满足约束的条件下得到最优的充放电功率, 而且所提出的改进 PPO 算法能够使智能体在选择动作时兼顾收敛性和探索性。


本文尽管成功将深度强化学习理论引入串联型微电网的控制中，但仅考虑了拓扑结构的串联特性。为充分发挥串联型微电网的特点和优点，后续还需进一步研究多智能体技术在串联型微电网控制中的应用，例如利用储能提升系统稳定性、功率协调控制等方面。

参考文献:

- [1] Wang Xinggui, Ding Yingjie, Li Jinjian, et al. Characteristics analysis of micro-source half-bridge converter series Y-connection based microgrid systems[J]. Journal of Power Electronics, 2023, 23(10): 1483-1495.
- [2] 胡维昊, 曹迪, 黄琦, 等. 深度强化学习在配电网优化运行中的应用[J]. 电力系统自动化, 2023, 47(14): 174-191.
Hu Weihao, Cao Di, Huang Qi, et al. Application of Deep Reinforcement Learning in Optimal Operation of Distribution Network[J]. Automation of Electric Power Systems, 2023, 47(14): 174-191(in Chinese).
- [3] 张自东, 邱才明, 张东霞, 等. 基于深度强化学习的微电网复合储能协调控制方法[J]. 电网技术, 2019, 43(6): 1914-1921.
Zhang Zidong, Qiu Caiming, Zhang Dongxia, et al. A Coordinated Control Method for Hybrid Energy Storage System in Microgrid Based on Deep Reinforcement Learning[J]. Power System Technology, 2019, 43(6): 1914-1921(in Chinese).
- [4] Bui V H, Hussain A, Kim H M. Double Q-learning-based distributed operation of battery energy storage system considering uncertainties[J]. IEEE Transactions on Smart Grid, 2020, 11(1): 457-469.
- [5] 刘俊峰, 陈剑龙, 王晓生, 等. 基于深度强化学习的微能源网能量管理与优化策略研究[J]. 电网技术, 2020, 44(10): 3794-3803.
Liu Junfeng, Chen Jianlong, Wang Xiaosheng, et al. Energy Management and Optimization of Multi-energy Grid Based on Deep Reinforcement Learning[J]. Power System Technology, 2020, 44(10): 3794-3803(in Chinese).
- [6] Ding T, Zeng Z Y, Bai J W, et al. Optimal electric vehicle charging strategy with Markov decision process and reinforcement learning technique[J]. IEEE Transactions on Industry Applications, 2020, 56(5): 5811-5823.
- [7] Cao D, Hu W H, Xu X, et al. Deep reinforcement learning based approach for optimal power flow of distribution networks embedded with renewable energy and storage devices[J]. Journal of Modern Power Systems and Clean Energy, 2021, 9(5): 1101-1110.
- [8] Qiu X, Nguyen T A, Crow M L. Heterogeneous energy storage optimization for microgrids[J]. IEEE Transactions on Smart Grid, 2016, 7(3): 1453-1461.
- [9] Kuznetsova E, Li Y F, Ruiz C, et al. Reinforcement learning for microgrid energy management[J]. Energy, 2013, 59(59): 133-146.
- [10] Wang S Y, Du L, Fan X Y, et al. Deep reinforcement scheduling of energy storage systems for real-time voltage regulation in unbalanced LV

- networks with high PV generation[J]. IEEE Transactions on Sustainable Energy, 2021, 12(4): 2342-2352.
- [11] Williams R J. Simple statistical gradient-following algorithms for connectionist reinforcement learning[J]. Machine Learning, 1992, 8(3): 229-256.
- [12] Schulman J, Levine S, Moritz P, et al. Trust region policy optimization[EB/OL]. (2015-02-19)[2024-07-21]. <http://arxiv.org/abs/1502.05477>.
- [13] Schulman J, Wolski F, Dhariwal P, et al. Proximal policy optimization algorithms[EB/OL]. (2017-07-20)[2024-07-21]. <http://arxiv.org/abs/1707.06347>.
- [14] Wang Xinggui, Li Jinjian, Guo Qun, et al. Parameter design of half-bridge converter series Y-connection microgrid grid-connected filter based on improved PSO-LSSVM[J]. International Transactions on Electrical Energy Systems, 2023: 9534004.
- [15] 邹伟, 高玲, 刘昱构. 强化学习[M]. 北京:清华大学出版社, 2020.
- Zou Wei, Ge Ling, Liu Yubiao. Reinforcement learning[M]. Beijing: Tsinghua University Press, 2020(in Chinese).
- [16] 秦湖程, 黄炎焱, 陈天德, 等. 基于 PPO 算法的集群多目标火力规划方法[J/OL]. 系统工程与电子技术.
- Qin Hucheng, Huang Yanyan, Chen Tiande, et al. Cluster multi-objective fire planning method based on PPO algorithm[J/OL]. Systems Engineering and Electronics(in Chinese).
- [17] 刘畅, 卓建坤, 赵东明, 等. 利用储能系统实现可再生能源微电网灵活安全运行的研究综述[J]. 中国电机工程学报, 2020, 40(1): 1-18.
- Liu Chang, Zhuo Jiankun, Zhao Dongming, et al. A review on the utilization of energy storage system for the flexible and safe operation of renewable energy microgrids[J]. Proceedings of the CSEE, 2020m 40(1): 1-18(in Chinese).

作者简介:

| | |
|---|---|
|  | 第一作者: 李锦键(1995), 男, 中国电源学会学生会员, 博士研究生, 研究方向为可再生能源发电系统与控制、微电网技术, E-mail: lijianjian0326@163.com。 |
| | 第二作者(通信作者): 王兴贵(1963), 男, 教授, 博士生导师, 研究方向为可再生能源发电系统与控制、微电网技术、电力电子与电力传动等, E-mail: wangxg8201@163.com。 |
| | 第三作者: 丁颖杰(1992), 女, 中国电源学会学生会员, 博士研究生, 研究方向为可再生能源发电系统与控制、微电网技术, E-mail: dingyj0820@126.com。 |
| 李锦键 | |